Versatile gamma-tubulin complexes contribute to the dynamic organization of MTOCs during *Drosophila* spermatogenesis

Elham Alzyoud[1#], Dóra Németh[1,2#], Viktor Vedelek[1], Titanilla Szögi[3], Viktória Petra Tóth[1], Mónika Krecsmarik[1], Edit Ábrahám[4,5], Zoltán Lipinszki[4,5*], Rita Sinka[1*]

[1]Department of Genetics, University of Szeged, Szeged, Hungary
[2]Faculty of Science and Informatics, Doctoral School of Biology, University of Szeged, Szeged, Hungary
[3]Department of Pathology, University of Szeged, Szeged, Hungary
[4]Synthetic and Systems Biology Unit, Institute of Biochemistry, HUN-REN Biological Research Centre, HUN-REN, Szeged, Hungary.
[5]National Laboratory for Biotechnology, Institute of Genetics, HUN-REN Biological Research Centre, Szeged, Hungary.

# These authors contributed equally to this work
* Authors for correspondence (rsinka@bio.u-szeged.hu, lipinszki.zoltan@brc.hu)

Abstract

The initiation of microtubule formation is facilitated by γ-tubulin and γ-Tubulin Ring Complex (γ-TuRC) in various microtubule-organizing centers (MTOCs). While the heterogeneity of tissue-specific MTOCs and γ-TuRC in *Drosophila* testis has been described, their molecular composition and physiological significance are poorly understood. We investigated the testis-specific distribution and biochemical interaction of the canonical γ-TuRC proteins Grip163 and Grip84. We found that while Grip163 is present on the centrosome and basal body, Grip84 localizes to the centrosome and Golgi in spermatocytes and colocalizes with the testis-specific γ-TuRC at the basal body, apical nuclear tip, and near the elongated mitochondria after meiosis. We also show the apical nuclear tip localization of some γ-TuRC interacting partners and prove their binding to testis-specific γ-TuRC proteins. These results highlight and prove the importance of the different γ-TuRCs in organizing the diverse MTOCs present during the extensive rearrangement of cell organelles during the spermatogenesis of *Drosophila*.

Introduction

The microtubule (MT) network in eukaryotic cells plays a crucial role in cell differentiation and division, as well as in the movement through the cilia and flagella. The spatial re-organization of the MT cytoskeleton is a fast and dynamic process that requires distinct subcellular nucleation sites called microtubule organizing centers (MTOCs) that act as templates for the MT arrays to initiate. The main MTOC in dividing cells is the centrosome, which consists of a pair of centrioles (an older mother and a newer daughter centriole), and the pericentriolar material (PCM). Apart from the centrosome, non-centrosomal microtubular organizational centers (ncMTOCs) are present in different cell types, but it is not known how these structures regulate the organization and dynamics of microtubules. The heterogeneity of ncMTOCs is reflected in the molecular composition and the cellular localization, and their function is unique to each cell type [1].

MTs are polar structures containing plus and minus end. The highly dynamic plus end is generally where the majority of MT polymerization and depolymerization occurs, while the minus end is often stabilized and capped [2]. The main factor known to specifically associate with microtubule minus ends is the γ-tubulin ring complex (γ-TuRC) [3,4]. PCM and ncMTOCs both recruit γTuRCs to the microtubule nucleation site [5,6]. γTuRC is a multiprotein complex consisting of γ-tubulin and its associated proteins (γ-tubulin ring proteins (Grips) in Drosophila, or γ-tubulin complex proteins (GCPs) in human) that are essential for γTuRC integrity and MT nucleation activity. The conserved and essential core of the γTuRC is the small complex (γTuSC) that consists of two γ-tubulins, one copy of Grip84 (human GCP2) and Grip91 (human GCP3) in Drosophila [7]. The large ring complex comprises multiple γ-TuSCs and additional Grips, including Grip75 (human GCP4), Grip128 (human GCP5), Grip163 (human GCP6), and Grip71 (NEDD1) [8,9]. An additional component of the microtubule nucleation machinery is Mzt1, which can bind to both γ-TuSC and γ-TuRC in many eukaryotes[10–12]. Although Mzt1 is essential in most organisms, it exhibits testis-specific expression and binds to Grip91 and t-Grip91 in *D. melanogaster*[13,14]. It was shown that γTuRC genes are not essential for viability, but γTuRC is able to nucleate microtubule organization more efficiently than the small complex alone [9].

Similarly to mammals, Drosophila spermatogenesis involves a series of stage-dependent morphological changes when stem cells give rise to mature sperm. During this process, round spermatids of 10 μm in diameter elongate to become 1850 μm in length [15], which requires an extensive remodelling of existing cellular organelles, as well as the addition of new structures. After meiosis, each spermatid inherits a

67 centriole that will serve a basal body around a ring-shaped PCM-like macromolecular structure called the
68 centriole adjunct. The growth of the axoneme starts from the basal body and continues to elongate towards
69 the spermatid tail **(Figure 1 a)**[16]. Opposite to the basal body, on one side of the nucleus, the acroblast
70 starts to develop, which is a Golgi-derived organelle. During the later stages of elongation, the acroblast
71 will be converted into the acrosome. Another important event that occurs after meiosis is the fusion of the
72 mitochondria into two giant mitochondrial derivatives, called the nebenkern. These mitochondrial
73 derivatives elongate with the axoneme during sperm maturation and accumulate paracrystalline material
74 in one of them, which could provide structural support for the growing tail **(Figure 1 a)**[15,17].
75 Growing evidence suggests that testis-specific MTOC components play important roles in basal body and
76 ncMTOC formation and also in the positioning and shaping of the post-meiotic organelles during
77 Drosophila spermatogenesis [13,14,18]. For instance, testis-specific CnnT expression contributes to the
78 conversion of mitochondria into a ncMTOC, independent of core pericentriolar Cnn [18]. In addition to the
79 canonical γ-TuRC genes (Grip84, Grip91, Grip75, Grip128, Grip163, and Grip71), we have recently
80 identified three additional testis-specific paralogs of the γ-TuRC components, t-Grip84, t-Grip91, and t-
81 Grip128 [14,19]. We have shown, that from the round spermatid stage onward, these t-γ-TuRC proteins start
82 to localize to the centriole adjunct, then to the nuclear tip, and finally surrounding the mitochondria of the
83 elongating cyst. We also presented that they bind to γ-Tubulin and Mzt1 and interact with each other in
84 the post-meiotic stages [14]. We and others have shown that Mzt1 binds to the N-termini of Grip/GCP
85 proteins and interacts with the N-terminal regions of Grip91, t-Grip91 and Grip128 in Drosophila [13,14].
86 Our finding raised the question of whether the canonical γ-TuRC proteins are replaced with their testis-
87 specific counterparts, or whether they are able to cooperate to meet the needs of microtubule nucleation
88 during the late stages of spermatogenesis. We also aimed to understand whether the testis-specific γ-TuRC
89 can interact with the canonical γ-TuRC or with any other proteins. In order to address these questions, we
90 created *in situ* tagged *Grip163* and *Grip84* transgenic lines to elucidate the adaptable localization and
91 identify interacting partners of the γ-TuRC during the development of male germ cells.
92
93 **Results**
94 **Phenotypic characterization of the *Grip163*$^{\Delta 11}$ mutant line**
95 We have reported previously that t-γ-TuRC proteins are present only in the post-meiotic spermatids [14].
96 However, there is a lack of data regarding the relationship between the canonical and the testis-specific γ-

97 TuRCs, as well as the presence or localization of ubiquitously expressed γ-TuRC components in the late
98 stages of spermatogenesis.
99 Therefore, we tested the presence and possible function of the γ-TuRC component Grip163, which has no
100 testis-specific paralogs, in sperm development [20,8,14]. To achieve this, we induced mutation in the *Grip163*
101 gene, and performed an *in situ* tagging of the *Grip163* gene, using the CRISPR-Cas9 gene editing
102 technology. Using a specific guided RNA designed for *Grip163*, we deleted 11 base pairs from the coding
103 region of the gene (hereafter, $Grip163^{\Delta 11}$). This deletion caused a frameshift leading to a premature stop
104 codon in the coding region of *Grip163* (**S.Figure 1a**). Interestingly, we found that in contrast to the G*rip84*
105 and *Grip91* homozygotes, which are lethal [21,22], the homozygous $Grip163^{\Delta 11}$ mutant animals are viable,
106 but male and female sterile (**S.Figure 1c).** It is known that the γ-TuSC is essential for centrosome
107 formation, mutants of the canonically expressed γ-TuRC components, *Grip128* and *Grip75,* are viable
108 and similar to $Grip163^{\Delta 11}$ male and female sterile [23,9,21,24,25]. The previously characterised $Dgrip163^{GE27087}$
109 mutant allele is male fertile and female sterile[9], therefore we decided to test the spermatogenesis phenotype
110 of $Grip163^{\Delta 11}$. $Grip163^{\Delta 11}$ is male and female sterile in hemizygous combination with the overlapping
111 *Df(3L)BSC574* deficiency, suggests that $Grip163^{\Delta 11}$ is a strong hypomorph or a null allele (**S.Figure 1c)**.
112 The seminal vesicles of the $Grip163^{\Delta 11}$ males were empty, without mature sperms (**Figure 1 b-c**). Based
113 on this phenotype we investigated both the early and late stages of spermatogenesis in $Grip163^{\Delta 11.}$flies.
114 We found an abnormal nebenkern-nucleus ratio in the round spermatids, which is a hallmark of abnormal
115 mitotic division (**Figure 2 a-c)**. Nevertheless, many of the cysts are able to elongate in the $Grip163^{\Delta 11}$
116 mutant, visualized by the β2tub-GFP transgene (**Figure 1 b, c)**. To further investigate the elongation of
117 the cysts, we tested whether the individualization proceeds normally. After the elongation of the cyst, an
118 actin rich cytoskeletal structure, the individualization complex (IC) is formed at the caudal end of the
119 nuclei surrounding the basal-body and axoneme. During individualization the IC moves towards the tip
120 of the tail, expelling and degrading all the cytoplasmic content from the spermatid and tightly cover the
121 axoneme-mitochondria complex with an individual plasma membrane **(Figure 1 a)**[26]. To visualize the
122 elongated post-meiotic cysts, we stained the actin cones of the IC in the $Grip163^{\Delta 11}$ testis and found the
123 lack of them in $Grip163^{\Delta 11}$, providing evidence for the failure of proper cyst elongation, which is the
124 prerequisite of individualisation **(Figure 1 d, e).** For further evidence, we used anti-pan polyglycylated
125 tubulin (Axo49) antibody to visualize mature axonemes of the spermatids, at the onset of individualization
126 [27]. We observed significantly shorter axonemes in the $Grip163^{\Delta 11}$ mutant compared to the wild-type (WT),
127 indicating abnormal spermatid elongation **(Figure 1 f-h).**

128 Axoneme elongation depends on the mitochondria, which provide a structural platform for MT
129 reorganization to support the robust elongation taking place at the tail tip of the sperm[28]. Based on this we
130 tested the presence and appearance of late elongating mitochondria using dj-GFP as a marker. In
131 accordance with the defect observed in axoneme elongation, it was detected that the mitochondria in the
132 *Grip163*$^{\Delta 11}$ mutants also exhibited incomplete elongation (**Figure 1 f-g**).
133 Based on this general spermatid elongation defect of *Grip163*$^{\Delta 11}$ flies, the detailed morphology of post-
134 meiotic cysts was further investigated using transmission electron microscopy (TEM). In wild-type testis,
135 the 64 spermatids develop simultaneously and on the TEM image of elongated cysts we observed the two
136 mitochondrial derivatives attached to the axoneme, which has the classical 9+2 arrangement of
137 microtubules in each spermatid (**Figure 2 d-f**). In *Grip163*$^{\Delta 11}$ mutants, cysts became disorganized, with
138 fewer spermatids per cyst and with disturbed mitochondrial:axonemal ratio (**Figure 2. e**). Frequently,
139 multiple mitochondrial derivatives were attached to a single axoneme **(Figure 2 g)**, and we also observed
140 multiple damaged axonemes **(Figure 2 h)**, supporting that Grip163 is necessary for normal axoneme
141 formation and/or stability. Since the γ-TuRC was proposed to be essential for centrosome formation in
142 somatic cells [11], we examined the centrosome/basal body distribution at different stages of
143 spermatogenesis in the testes of *Grip163*$^{\Delta 11}$ males. We tested the presence and the distribution of the
144 centrosomal/basal body localized γ-Tubulin and the PACT domain of DPlp fused with GFP (GFP-PACT)
145 [29]. In the wild-type animals both proteins localize to the centrosome/basal body during different stages of
146 spermatogenesis **(Figure 3 a-b, S.Figure 2b)**. In wild-type males, GFP-PACT is located close to the
147 nucleus and the nebenkern, as expected in round spermatids. In contrast, multiple and scattered GFP-
148 PACT signals were observed in the *Grip163*$^{\Delta 11}$ mutants' testis (**Figure 3 c-d, S.Figure 2b-c)**. We
149 calculated both the nucleus-nebenkern and the basal body-nebenkern ratio in the round spermatids
150 **(S.Figure 2a)**. Theoretically, these ratios should be close to 1 in WT, as each spermatid is supposed to
151 have one of each organelles per cell. However, we found that the *Grip163*$^{\Delta 11}$ mutant were significantly
152 different from the expected 1. In the *Grip163*$^{\Delta 11}$ mutant, the average ratio is higher than one (~2.06, ~2.01)
153 indicating that there are less nebenkerns but approximately equal amount of basal bodies and nuclei
154 **(S.Figure 2a)**. These abnormalities could be the consequence of cytokinetic defects of the meiotic cysts
155 of *Grip163*$^{\Delta 11}$ mutant.
156 We also measured the fluorescence intensity of γ-Tubulin and GFP-PACT in premeiotic and post-meiotic
157 cysts. Both in WT and the *Grip163*$^{\Delta 11}$ mutant flies we found strong GFP-PACT positive centrosomal and

158 basal body signals **(Figure 3 c-d)**, however, the γ-Tubulin signal was weak in spermatocytes compared to
159 the WT spermatocytes **(S.Figure 2d-e)**.
160 Surprisingly, after meiosis the γ-Tubulin signal was stronger and accumulated on the basal body both in
161 WT and *Grip163*$^{\Delta 11}$ mutant spermatids, but those were scattered along the cysts (**Figure 3 c, d**, **S.Figure**
162 **2e)**. It was previously proposed that γ-Tubulin could be recruited to the centrosomes in somatic cells by
163 γ-TuSCs, independently of the γ-TuRCs [9]. Mzt1 is a well characterised binding partner of the γ-TuSC and
164 we showed previously, that the post-meiotically localizing three t-Grip proteins (t-Grip84, t-Grip91, t-
165 Grip128) bind to γ-Tubulin and t-Grip91 and also to Mzt1 [14,30]. The γ-TuRC interacting Mzt1 is localised
166 to the centrosome, basal body and the surface of the mitochondria from the meiotic stages onward and
167 also to the apical tip of the elongating nuclei **(Figure 9)** [14]. We found Mzt1 localization on the surface of
168 the mitochondria in *Grip163*$^{\Delta 11}$ mutant, suggesting that Grip163 and probably γ-TuRC are not essential
169 for Mzt1 mitochondrial anchoring. Similar to γ-Tubulin, Mzt1 is not present on the meiotic basal body,
170 however, in the post-meiotic stages, it localizes to the dispersed basal body in the *Grip163*$^{\Delta 11}$ mutant
171 spermatids **(S.Figure 3).** All these data suggest that Grip163 could be essential for the formation of stable
172 γ-TuRC before and at the onset of meiosis, however, the newly organized testis-specific γ-TuRC could
173 contribute to the γ-Tubulin and Mzt1 binding after meiosis **(Figure 9)**.
174
175 **Localization of γ-TuRC proteins during spermatogenesis**
176 To test the subcellular localization of Grip163 at different stages of spermatogenesis, we generated
177 endogenously GFP-tagged Grip163 transgenic lines. We and others have shown that the N- or C-termini
178 of the γ-TuRC proteins are responsible for the binding of their interacting partners [13,14], therefore we
179 tagged the Grip163 close the N-terminus (aa150) (**S.Figure 1)**, without interfering with the functional
180 GCP domains of the protein (**S.Figure 1 a**). The fertility of the GFP-Grip163 males is comparable to the
181 wild-type animals, indicating that the inserted fluorescent tag does not alter the function of the protein
182 (**S.Figure 1 c)**. GFP-Grip163 signal is present and colocalised with γ-Tubulin on the centrosomes and
183 basal body on the developing spermatids **(Figure 4 a-b)**.
184 We also showed the colocalization of GFP-Grip163 with γ-Tubulin and also with HA-t-Grip91 on the
185 post-meiotic basal body/centriole adjunct **(Figure 4 c-d)**. These results strongly suggest that the testis-
186 specific γ-TuRC does not replace the canonical γ-TuRC, but both are present on the basal body/centriole
187 adjunct of the developing spermatids **(Figure 9)**.

188 The localization of GFP-Grip163 to the post-meiotic centriole adjunct has prompted an inquiry into the
189 potential presence of other canonical γ-TuSC components in the subsequent developmental stages. To
190 investigate this, we applied CRISPR technology to *in situ* tag Grip84 with GFP. We designed the
191 incorporation in a way that all 5 potential isoforms of Grip84 will have the N-terminally inserted GFP tag,
192 outside of the GCP domain (**S.Figure 1 b**). It was previously reported that the classical mutant of *Grip84*
193 is lethal, therefore the normal viability and fertility of the *in situ* GFP-tagged Grip84 serves as evidence
194 that the GFP tag does not alter the normal function of Grip84 (**S.Figure 1 c**) [31]. We found that GFP-Grip84
195 is present on the centrosomes of spermatocytes, similarly to the GFP-Grip163 protein (**Figure 5 a-e**). This
196 localization of GFP-Grip84 was also verified by its colocalization with the centrosomal component
197 Asterless (Asl) (**Figure 6 a, S.Figure 4 a, b, Figure 9**) [32].
198 Following meiosis, GFP-Grip84 is present on the centriole adjunct and then appears at the apical nuclear
199 tip and exhibits a strong overlap with the elongated mitochondria, akin to the GFP-Grip163. We wanted
200 to know whether the post-meiotic localization of GFP-Grip84 overlaps with its testis-specific paralogue,
201 t-Grip84. To do this we co-expressed GFP-Grip84 and t-Grip84-mCherry together and found complete
202 colocalization after the meiotic stages (**Figure 5 f, g**) [14]. These results provide additional evidence that
203 both the ubiquitously expressed γ-TuRC and the testis-specific γ-TuRC may collectively contribute to the
204 formation of the diverse microtubule organizing centers during the post-meiotic stages of spermatids.
205 Apart from the centrosomal localization of GFP-Grip84, we also noticed strong bright punctae in the
206 cytoplasm of spermatocytes, whose distribution is reminiscent of t-ER-Golgi units. It is known that
207 centrosomal proteins are associated with the Golgi apparatus in mammalian cells [33]. Golgi organization is
208 special in Drosophila, as the scattered Golgi stacks are found in close proximity to the ER exit sites (t-ER-
209 Golgi) [34]. To test the t-ER-Golgi localization of GFP-Grip84, we used GM130 as a *cis*-Golgi, as well as
210 GCC88, as a *trans*-Golgi-specific antibody for co-immunostaining (**Figure 6 b-e, S.Figure 4 c-d, Figure**
211 **9**). We observed strong co-localization of GFP-Grip84 with the *cis*-Golgi, suggesting that GFP-Grip84 is
212 connected to the t-ER-Golgi units of spermatocytes.
213 In a comprehensive analysis of the effector proteins of Rab GTPases, Grip84, Grip91 and γ-Tubulin were
214 identified as interacting partners of the Golgi-localizing Rab2 and Rab4 [35]. Rab2A and Rab2B proteins
215 were shown to be essential for acrosome formation and male fertility in mice [36], therefore it seemed
216 reasonable to check whether the Golgi-localizing Rab2 might also be present at the apical end where the
217 acrosome is located during nuclear elongation in Drosophila spermatids. We tested the germline-specific
218 Bam-Gal4 driven pUASP-Rab2-YFP localization in spermatocytes and spermatids. We detected Rab2-

219 YFP on the t-ER-Golgi units adjacent to the *trans*-Golgi-specific antibody GCC88 in spermatocytes and
220 on the acrosome containing apical nuclear tip of the elongated spermatids (**Figure 6 d, e**). Localization of
221 GFP-Grip84 to the Golgi apparatus led us to hypothesize that Drosophila γ-TuRC, similarly to the
222 mammalian γ-TuRC might be necessary to the Golgi organization and also could have a possible function
223 of Rab2 in acrosome formation **(Figure 9)**. Additional experiments can address these highly intriguing
224 prospects.
225
226 **Post-meiotic ncMTOCs contain centrosomal components**
227 The versatile localization pattern of GFP-Grip84 prompted us to investigate whether any of the already
228 known binding partners of the γ-TuRC could be present on the newly identified localization foci. It was
229 shown previously that γ-Tubulin is localized in the apical region of the spermatid nuclei, specifically at
230 the distal end of the MTs present within the dense complex [14,37]. We have previously demonstrated the
231 presence of t-γ-TuRC and Mtz1 at the apical tip of the nucleus, suggesting the presence of a ncMTOC
232 organized opposite to the basal body during nuclear elongation [14]. Therefore, we carefully examined the
233 precise localization of the centriole component, Sas4, a known interacting partner of γ-TuRC proteins by
234 immunostaining using anti-Sas4 antibody [38,39]. We detected Sas4 on the centrosome of mitotic
235 spermatocytes and the basal body of the spermatids after meiosis (**Figure 7 a-c**). Intriguingly, we detected
236 endogenous Sas4 on the apical tip of the elongating spermatid nuclei as well (**Figure 7 c**). Apart from the
237 γ-TuRC proteins, Sas4 has multiple centriolar binding partners, including Sas6, Asl, Ana1, and Dplp [32,39–
238 42]. Therefore, we wondered whether they are also present on the site, which has been suggested as a
239 ncMTOC at the apical tip of the spermatid nuclei. To achieve this we performed immunostainings using
240 gene-specific antibodies [32,38,43].
241 We detected Sas6 and Asl at the centriole adjunct and also at the apical tip of the nuclei (**S.Figure 5 a, b**),
242 however, Ana1 and GFP-PACT colocalized with t-Grip91 exclusively at the centriole adjunct region of
243 the elongating leaf and canoe stage nuclei, in line with the reported localization pattern of these proteins
244 (**Figure 7 d, S.Figure 5 c**) [37]. These results indicate that the site which has been suggested as a ncMTOC
245 at the apical nuclear tip contains several well-defined binding partners of the γ-TuRC **(Figure 9)**.
246
247 **Composition of t-γ-TuRC**
248 We next examined whether the partially overlapping localization pattern might be a consequence of the
249 physical interaction between the canonical γ-TuRC and the t-γ-TuRC and/or the t-γ-TuRC proteins and

250 the γ-TuRC interacting protein Sas4. To address this, we performed a yeast two-hybrid (Y2H) analysis,
251 where we tested t-γ-TuRC proteins with the canonical γ-TuRC protein Grip91, Grip84, Grip163, Grip75
252 and Sas4. Due to the large size of these proteins, we split all three t-γ-TuRC proteins as well as Grip91,
253 Grip163 and Grip128 into an N-terminal (NT) and a C-terminal (CT) part. Grip84, Grip75 and Sas4 were
254 used as full-length **(S.Figure 6a)**. A specific interaction was found between t-Grip84-CT and Grip91-NT,
255 which suggests the possibility of the presence of a testis-specific and non-testis-specific mixed γ-TuRC
256 (**Figure 8 a, S.Figure 6-7**). We also detected interaction between t-Grip84-CT and Grip84, between t-
257 Grip91-NT and Grip84, Grip91-CT, Grip75, Grip163-NT, Grip163-CT and finally between t-Grip91-CT
258 and Grip84, Grip91-CT, Grip75, Grip163-NT, Grip163-CT. Sas4 was able to bind to and t-Grip91-NT, t-
259 Grip91-C, t-Grip128-N and t-Grip128-C however, we could not find an interaction between Sas4 and t-
260 Grip84-N, t-Grip84-C (**Figure 8 a, S.Figure 6-7**).
261 To support Y2H results and prove the direct interaction between proteins, we performed an *in vitro* binding
262 experiment and tested several combinations of proteins that showed interaction in the Y2H assay. We used
263 immobilised GST-tagged recombinant proteins (N- or C-terminal parts of the t-γ-TuRC proteins, as
264 indicated) as bait, which were mixed with ^{35}S-methionine-labelled Sas4 or Grip91, respectively, produced
265 by a coupled *in vitro* transcription-translation (IVTT) reaction followed by autoradiography (**Figure 8 b-**
266 **e, S.Figure8**). The *in vitro* binding experiments confirmed the results of the Y2H assay (**Figure 8 a-e**).
267 Both the localisation and the interaction studies suggest the presence of different γ-TuRC/t-γ-TuRC
268 complexes coexisting. To further investigate these complexes, we conducted biochemical isolation and
269 analysis of the subunit composition and migration pattern of various γ-tubulin-containing complexes in
270 testis samples. This involved fractionating protein complexes from testes extracts using Superose 6 size-
271 exclusion chromatography (SEC) [44]. As a control, we fractionated canonical γ-Tubulin complex
272 components from embryo extract (0-5 hours embryos contain somatic centrosomal MTOCs with canonical
273 γ-TuRC, but without t- γ-TuRC proteins) of the γ-TuSC component GFP-Grip84 and γ-TuRC component
274 GFP-Grip163, and probed them with anti-GFP, anti-γ-Tubulin and anti-p54 antibodies **(S.Figure 9)**. To
275 estimate the relative molecular weights of the analysed protein complexes, we compare them to the SEC
276 profile of p54/Rpn10, the ubiquitin receptor subunit of the 2,5 MDa 26S Proteasome[45]. The same
277 extraction and fractionation method was used to analyse testes extracts by SEC, and to investigate the
278 presence of different t- γ-TuRC in each fraction. We analysed GFP-Grip163 and GFP-Grip84, γ-Tubulin
279 and members of the testis-specific complexes, HA-t-Grip91 and t-Grip84-mCh. Their SEC profiles

280 suggest that they co-migrate in the high molecular weight fractions, and partially co-migrate (their peaks
281 partially overlap) in the low molecular weight fractions **(S.Figure 9)**.
282
283
284 **Discussion**
285 Drosophila spermiogenesis and spermatogenesis represent an ideal model for studying mitotic and meiotic
286 cell division, centrosome and basal body formation and dynamic organelle reorganization after meiosis.
287 It was proven to be a good model for understanding centrosomal and non-centrosomal MT nucleation due
288 to the intensive morphological changes and organelle movement in the post-meiotic spermatids [13,14,18].
289 MT nucleation was reported, among others, at the surface of the Golgi [46], mitochondria [18], nuclear
290 envelope [47] and plasma membrane [48] in mammalian cells. We previously identified and described the
291 function and versatile localization of three testis-specific γ-TuRC proteins in the post-meiotic spermatids
292 [14](**Figure 9**). The described centriole adjunct, nuclear tip and mitochondrial surface localization of the t-
293 γ-TuRC proteins and their interaction partner Mzt1 raised the question of whether the ubiquitously
294 expressed γ-TuRC is replaced after meiosis for the testis-specific one or both are present due to the
295 multiple putative ncMTOC formation during spermatid elongation and acrosome formation. γ-Tubulin
296 was already reported to localize to both tips of the elongating nuclei and to the surface of the giant
297 mitochondria during elongation [14,18,37]. The testis-specific splice variant of Centrosomin (Cnn), CnnT, was
298 also reported to promote non-centrosomal MT growth on the surface of the mitochondrial derivative of
299 spermatids, and the N-terminal region of Cnn-T was shown to bind efficiently to γ-TuRCs, but there was
300 no data about the canonical γ-TuRC localization after the meiotic stages of spermatogenesis[18,49]. Mutants
301 for the small complex components Grip91 and Grip84 are lethal and have defects in spindle assembly [21,22],
302 which indicates their essentiality for the whole fly development. It has been demonstrated that the small
303 complex is the minimal unit needed for MT nucleation [7]. However, RNAi depletion of the ubiquitously
304 expressed Grip163 results in loss of Grip84 recruitment to the ncMTOC in tracheal cells [9].
305 Our experiments showed that, in contrast to the essentiality of the γ-TuSC, the γ-TuRC member Grip163
306 is only essential for fertility, similar to the already characterized γ-TuRC members Grip75 and Grip128
307 [23]. From the elongation and basal body stability defects of *Grip163* mutant spermatids, we inferred that
308 the presence of Grip163 protein is essential after meiosis. This was supported by the localization of GFP-
309 Grip163, as we detected its presence in the localization foci of t-γ-TuRC members after meiosis. These
310 results raised the possibility that t-γ-TuRC and the canonical γ-TuRC may be present simultaneously, even

311 as a mixed complex, in the aforementioned possible ncMTOCs (**Figure 9**). This hypothesis was further
312 supported by the fact that Grip84, a member of γ-TuSC, also exhibits an overlapping localization pattern
313 in the late stages of spermatogenesis and the physical interaction between t-Grip84 and the ubiquitously
314 expressed Grip91. Our results strongly suggest that both testis-specific and canonical γ-TuRC members
315 are involved in the formation of post-meiotic ncMTOCs. Although we observed very similar enrichment
316 patterns in testis samples, they were not identical to those of the embryo samples. The variation can be
317 elucidated by the distinct MTOCs found at various developmental stages and in diverse localization sites
318 within the testis, each characterized by unique or shared protein compositions of gamma-tubulin
319 complexes. Nevertheless, the biochemical isolation of these MTOCs poses a significant challenge for
320 future studies. Considering both the *in vivo* localization patterns and the *in vitro* interaction findings, we
321 suggest a versatile composition of gamma-tubulin complex formation occurring at the basal body, on the
322 mitochondrial surface, and at the apical tip of the nucleus in Drosophila spermatids.
323 Based on the localization and mutant phenotype of canonical Grip163 and testis-specific t-Grips, it can be
324 assumed that the larger amount and diverse composition of gamma-tubulin complex is required for the
325 cellular reorganization of the elongating spermatids. Gamma-tubulin complexes could be essential to the
326 stable attachment of the basal body/centriole adjunct to the sperm nucleus and for the nucleation and
327 stabilization of tubulins contributing to the formation of the nearly 1,8 mm long axoneme and also to the
328 nucleation of the axoneme independent microtubules around the elongating mitochondrial
329 derivatives[13,14,28].
330 *In vivo* tagging of Grip84 enabled us to describe the Golgi localization of the γ-TuSC component Grip84
331 in primary spermatocytes, in addition to the extensively studied centrosomal localization of the Grip84 [22].
332 Until now γ-Tubulin containing Golgi outpost-associated MT nucleation sites was only described to
333 regulate distal dendritic branching in *Drosophila* neurons [50]. Golgi non-centrosomal MT assembly is
334 mediated by the γ-Tubulin-interacting AKAP450 protein, which is anchored by the cis-Golgi-associated
335 GM130 protein. This provides evidence that the Golgi apparatus may become a major site of MT
336 nucleation by acting as a γ-TuRC docking site in mammalian cells by a mechanism similar to that in the
337 centrosome [51]. Our results suggest that a similar mechanism could be present in the primary spermatocytes.
338 Further experiments are needed to determine exactly which isoform of the Grip84 protein is associated
339 with the Golgi (**Figure 9**).
340 All three proteins of γ-TuSC (Grip84, Grip91 and γ-Tubulin) interact with the constitutively active, GTP-
341 bound Rab2 protein [35], and Rab2 and Grip84 both localize to both the Golgi and the apical end of the

342 nucleus, suggesting a role for γ-TuSC and Rab2 in the formation of the Golgi and lysosome-associated
343 acrosome. Rab2A and Rab2B proteins were shown to be components of the proacrosomal membrane and
344 essential for acrosome formation and male fertility in mice [36].
345 Drosophila Rab2 is an essential gene and recruitment of Rab2 takes place on the membranes of late
346 endosomes, where it controls the fusion of LAMP-containing biosynthetic carriers and lysosomes to late
347 endosomes in somatic cells [52]. t-ER-Golgi units contribute to the formation of the acroblast, which forms
348 the acrosome by fusing lysosomal structures during nuclear elongation in Drosophila [53]. The molecular
349 determinants of acrosome formation are hardly known in Drosophila, however, several retrograde
350 tethering complexes were described in the formation of a functional Golgi ribbon in the acroblast (Fári et
351 al 2016). Acrosomal proteins such as Sneaky, Lamp1 and Rab2, as well as the ubiquitous and testis-
352 specific γ-TuRC, its partner proteins (Mzt1, Sas4) and other centrosomal proteins (Asl, Sas6), are all
353 localized to the apical tip of the nucleus. Further biochemical studies are needed to clarify the precise
354 interactions between the aforementioned proteins. Nevertheless, these results raise the possibility of a link
355 between the ncMTOC and acrosome organization, which is present at the dense complex forming
356 perinuclear MTs at the apical end of the nuclei (**Figure 9**).
357

358 **Materials and Methods**

359 **Fly stocks, mutants, and fertility test**

360 Flies were maintained on cornmeal agar medium at 25˚C in standard laboratory conditions. Fly stocks
361 used in this study were obtained from Bloomington Drosophila Stock Center, except stated otherwise:
362 w^{1118} used as wild-type control (3605, BDSC), w[1118];Df(3L)BSC574 (25125 BDSC), P{UASp-
363 YFP.Rab2.Q65L}02 (9760, BDSC), P{DJ-GFP.S}AS1/CyO (5417, BDSC). *bam*-Gal4 testis specific
364 driver [54] was used (kindly provided by Helen White-Cooper) to express Rab2 in the germline. The β2-
365 tubulin-GFP line was provided by David M. Glover. GFP-PACT line was obtained from Jordan Raff's [29].
366 Mzt1-GFP, HA-t-Grip91 and t-Grip84-mCh were described before [14].

367 To establish the mutant allele $Grip163^{\Delta 11}$ the pCFD5-Grip163-gRNA line was crossed with vas-Cas9
368 source line to generate deletion in *Grip163*. The deletions were identified by *Grip163* specific PCR and
369 further confirmed by direct sequencing. $Grip163^{\Delta 11}$ line was established and used for further analysis.

370 To establish the genomic tagged lines of *Grip84* and *Grip163* pCFD5-Grip84-gRNA and pCFD5-
371 Grip163-gRNA lines were crossed with the vas-Cas9 source lines , w[1118]; PBac{y[+mDint2]
372 GFP[E.3xP3]=vas-Cas9}VK00027 (BL51324), y[1] M{RFP[3xP3.PB] GFP[E.3xP3]=vas-Cas9}ZH-2A
373 w[1118]/FM7c (BL51323) respectively, progeny of this cross were injected with the homology arm
374 carrying pJET1.2 plasmid (Thermo Fisher Scientific). Transgenic candidates were identified by gene
375 specific PCR and confirmed by sequencing of the insertion sites. For fertility tests, individual males were
376 crossed with three w^{1118} virgin females. After 3 days the parents were removed and 14 days after crossing,
377 the hatched progeny was counted in every tube. Experiments were repeated 4 times with > 10 males per
378 condition.

379 **DNA constructs**

380 To make the genomic GFP-Grip84, and GFP-Grip163 line, annealed oligos of the sgRNAs
381 (ATCCTTGAGCGGCTACCGCT), (GTGCTTCTCCGGTCCAGGCT) for Grip84 and Grip163
382 respectively were ligated into pCFD5 vector (Addgene, 112645) at Bbs1 restriction site. To establish the
383 homology arms 1534bp upstream, 1529bp downstream, 1515bp upstream and 1738bp downstream of the
384 intended GFP insertion site for Grip84 and Grip163 respectively in addition to GFP were amplified using
385 High fidelity DNA polymerase. The purified PCR products were cloned into pJET1.2 plasmid (Thermo
386 Fisher Scientific) using HiFi DNA Assembly Master Mix (E2621S, NEB) [55]. GFP sequence was
387 introduced 187bp upstream for Grip84, and 229bp upstream of the Grip163 sgRNA. Stable transgenic
388 lines were established as described in Port et al. [56]; [57].

389 For Y2H analysis t-Grip84-NT (1-399 aa)[58] t-Grip84-CT (400-728 aa)[58], t-Grip128-NT (1-550 aa)[58], t-
390 Grip128-CT (551-975 aa)[58] and t-Grip91-NT (1-966 aa)[58], t-Grip91-CT (967-1932 aa)[58] were cloned into
391 pGAD424. Full-length of Sas4 (1-901 aa), Grip84 (1-833 aa (Grip84-PD)), Grip75 (1-650 aa) and Grip91-
392 NT (1-545 aa), Grip91-CT (546-917 aa), Grip163-NT (1-685 aa) Grip163-CT (686-1351 aa), Grip128-
393 NT (1-585 aa) Grip128-CT (586-1092 aa) were cloned into pGBT9, using HiFi DNA Assembly Master
394 Mix (E2621S, NEB). To generate GST-tagged bait proteins for the *in vitro* pull-down assay, full-length
395 Grip84, N- and C-terminal parts of t-Grip84, t-Grip91 and t-Grip128 were inserted into the pDEST15
396 (11802014, Thermo Fisher Scientific) vector by Gateway cloning (11791-020, Thermo Fisher Scientific).
397 Sas4 and Grip91 cDNAs were obtained from the *Drosophila* Gold collection (DGRC) and inserted into
398 the pDEST17 plasmid (11803012, Thermo Fisher Scientific) by Gateway cloning. Oligonucleotide
399 primers used in cloning are listed in **(S. Table 2)**.

400 **Staining and microscopy**

401 Preparation and staining of testes with formaldehyde or methanol:acetone fixation were performed as
402 described by White-Cooper *et. al* [59]. Briefly, testes were dissected and fixed in 4% formaldehyde for 25
403 minutes or semi-squashed using a coverslip on poly-L-lysine coated slides, then frozen with liquid
404 nitrogen and fixed for 5 minutes in ice-cold methanol followed by 5 minutes in acetone. After fixation
405 samples were blocked and antibodies were added, the antibodies used in the study are listed in **(S.Table**
406 **1)**. Stained samples were mounted in SlowFade Gold antifade reagent (S36967, Life Technologies).
407 Images were taken using Olympus BX51 fluorescent microscope or Olympus Fluoview Fv10i confocal
408 microscope.

409 Testes for transmission electron microscopy were dissected and fixed overnight at 4°C in 2%
410 paraformaldehyde and 2% glutaraldehyde. After rinsing in phosphate-buffered saline (PBS), the testes
411 were further fixed for 1 h in 2% OsO_4, followed by dehydration in increasing ethanol concentrations and
412 rinsing in uranyl acetate and acetone. The samples were embedded in Embed812 (Electron Microscopy
413 Sciences, Hatfield, PA, USA) then ultrathin (70 nm) sections were cut on an Ultracut S ultra-microtome
414 (Leica, Wetzlar, Germany), which were mounted on copper grids. The grids were counterstained with
415 uranyl acetate (Merck, Germany) and lead citrate (Merck, Germany) and were examined and
416 photographed with a JEOL JEM 1400 transmission electron microscope (JEOL, Tokyo, Japan). The
417 images were processed with the TEM Center software (JEOL, Tokyo, Japan).

418 **Yeast two-hybrid assay**

419 Y2H assays were carried out using the Matchmaker two-hybrid system (K1605, Clontech). One of the
420 baits pGBT9 was cotransformed with one of the preys pGAD424 into PJ69 yeast cells [60]. Individual
421 colonies were streaked out on yeast synthetic double drop-out plates that lacked tryptophan and leucine
422 (Y0750, Merck), after growing, they were inoculated on double and triple dropout plates lacking
423 (tryptophan, leucine, histidine, and adenine (Y2021, Merck) contains 5-10 mM 3-amino-1, 2,
424 4-aminotrizole (3-AT) (A8056, Sigma).

425 **Recombinant protein production**

426 Recombinant GST-tagged bait proteins were expressed, purified and immobilized onto glutathione
427 sepharose beads as described previously [61].

428 **Coupled *in vitro* transcription-translation (IVTT) reaction and *in vitro* binding assay**

429 ^{35}S-methionine-labelled prey proteins (Grip91, Sas4) were produced *in vitro* using the TnT T7 Quick
430 Coupled IVTT kit (L1170, Promega). The detailed protocol of the GST-IVTT binding assay is described
431 previously [62].

432 **Gel-filtration chromatography and western blotting**

433 Separation of gamma-tubulin-containing complexes were carried out by size exclusion chromatography
434 (SEC) based on the protocol published earlier [44] with slight modifications. All steps were conducted at
435 4°C or on ice unless otherwise stated. Briefly, 25 mg of 0-5 h old dechorionized embryos (expressing
436 GFP-Grip84 or GFP-Grip163) or 500 dissected testes (expressing HA-t-Grip91, t-Grip84-mCh, GFP-
437 Grip84, or GFP-Grip163, respectively) were homogenized in 350 µl HB buffer (50 mM K-HEPES pH
438 7.6, 75 mM KCl, 1 mM $MgCl_2$, 1 mM EGTA, 1 mM DTT, 1 mM PMSF, and EDTA-free protease inhibitor
439 cocktail (PIC, Roche, #11873580001)) using a Dounce homogenizer. Ten strokes with a loose pestle
440 followed by ten strokes with a tight pestle were applied, followed by further homogenization by a plastic
441 pestle in microfuge tubes for 5 min. The samples were centrifuged at 15,000 *xg* for 30 minutes at 4°C.
442 The supernatants were collected and centrifuged again at 21,000 *xg* for 10 minutes at 4°C. Three hundred
443 microliters of clarified lysates were subjected to SEC using a Superose 6 HR 10/30 FPLC column (Cytiva)
444 pre-equilibrated with HB buffer (without DTT, PMSF, and PIC). Forty-one fractions (0.3 ml each) were
445 collected after 7 ml. Ice-cold acetone (2.1 ml) was added to each fraction, the samples were vortexed, and
446 precipitation was carried out at -20°C for 24 hours followed by centrifugation at 17,000 *xg* for 30 minutes
447 at 4°C. The precipitated proteins were resolved in Laemmli sample buffer, boiled for 5 min, and loaded
448 onto SDS-PAGE, followed by western blot analysis using the indicated antibodies: anti-GFP mouse mAb
449 (1:1000, Roche, #11814460001), anti-mCherry rabbit mAb (1:1000, Abcam, #ab213511), anti-gamma-

tubulin mouse mAb (1:5000, Sigma, clone GTU-88, #T6557), anti-HA mouse mAb (1:40, Roche, clone 12CA5, #11583816001), and anti-p54/Rpn10 mouse mAb (1:400, [45]). The following secondary antibodies were used in western blot: goat anti-mouse IgG conjugated to horseradish peroxidase (1:10,000, Dako, #P044701-2) and goat anti-rabbit IgG conjugated to horseradish peroxidase (1:10,000, Dako, #P044801-2).

Quantification and statistical analysis

Nuclei and nebenkern were counted based on images taken by Olympus BX51. GFP-PACT signals and nebenkern were counted on living samples. GFP-PACT and γ-Tub intensity was measured by FV10-ASW Viewer software (Ver.4.2) on images taken with the same settings, fluorescence intensity was measured in the axis of PACT-GFP signal. Fluorescence intensity were adjusted based on background.

Data analysis and graph production was done using Origin 9.0 (OriginLab Corporation, Northampton, MA, USA). One-way ANOVA followed by Tukey's HSD test was used to comparisons between WT and mutants. Additional visualisation were made using Python 3.0 seaborn library.

Acknowledgements

We are grateful to all members of the Sinka lab. We are indebted to David M. Glover, Helen White-Cooper, Sean Munro and Jordan Raff for fly stocks and reagents; for the Drosophila Genomics Resource Center (supported by NIH grant 2P40OD010949) for cDNA clones and to Ferenc Jankovics for critical reading of the manuscript.

Funding

This work was supported by Hungarian Science Foundation (K132155) to RS and the National Laboratory for Biotechnology (2022-2.1.1-NL-2022-00008) to ZL.

Conflict of Interest

There is no conflict of interest.

475 **References**

476

477 1. Tillery, M., Blake-Hedges, C., Zheng, Y., Buchwalter, R. & Megraw, T. Centrosomal and
478 Non-Centrosomal Microtubule-Organizing Centers (MTOCs) in Drosophila melanogaster.
479 *Cells* **7**, 121 (2018).
480 2. Desai, A. & Mitchison, T. J. Microtubule polymerization dynamics. *Annu. Rev. Cell Dev.*
481 *Biol.* **13**, 83–117 (1997).
482 3. Moritz, M., Braunfeld, M. B., Guénebaut, V., Heuser, J. & Agard, D. A. Structure of the γ-
483 tubulin ring complex: A template for microtubule nucleation. *Nat. Cell Biol.* **2**, 365–370
484 (2000).
485 4. Zheng, Y., Wong, M. L., Alberts, B. & Mitchison, T. Nucleation of microtubule assembly by
486 a gamma-tubulin-containing ring complex. *Nature* **378**, 578–583 (1995).
487 5. Fry, A. M., Sampson, J., Shak, C. & Shackleton, S. Recent advances in pericentriolar
488 material organization: ordered layers and scaffolding gels. *F1000Research* **6**, 1622 (2017).
489 6. Kollman, J. M., Merdes, A., Mourey, L. & Agard, D. A. Microtubule nucleation by γ-tubulin
490 complexes. *Nat. Rev. Mol. Cell Biol.* **12**, 709–721 (2011).
491 7. Oegema, K. *et al.* Characterization of Two Related Drosophila γ-tubulin Complexes that
492 Differ in Their Ability to Nucleate Microtubules. *J. Cell Biol.* **144**, 721–733 (1999).
493 8. Gunawardane, R. N. *et al.* Characterization and reconstitution of Drosophila gamma-tubulin
494 ring complex subunits. *J. Cell Biol.* **151**, 1513–1524 (2000).
495 9. Vérollet, C. *et al.* Drosophila melanogaster gamma-TuRC is dispensable for targeting
496 gamma-tubulin to the centrosome and microtubule nucleation. *J. Cell Biol.* **172**, 517–528
497 (2006).

498 10. Tovey, C. A. & Conduit, P. T. Microtubule nucleation by γ-tubulin complexes and beyond.
499 *Essays Biochem.* **62**, 765–780 (2018).
500 11. Dhani, D. K. *et al.* Mzt1/Tam4, a fission yeast MOZART1 homologue, is an essential
501 component of the γ-tubulin complex and directly interacts with GCP3Alp6. *Mol. Biol. Cell*
502 (2013) doi:10.1091/mbc.e13-05-0253.
503 12. Masuda, H., Mori, R., Yukawa, M. & Toda, T. Fission yeast MOZART1/Mzt1 is an essential
504 γ-tubulin complex component required for complex recruitment to the microtubule
505 organizing center, but not its assembly. *Mol. Biol. Cell* (2013) doi:10.1091/mbc.e13-05-
506 0235.
507 13. Tovey, C. A. *et al.* γ-TuRC Heterogeneity Revealed by Analysis of Mozart1. *Curr. Biol. CB*
508 **28**, 2314-2323.e6 (2018).
509 14. Alzyoud, E., Vedelek, V., Réthi-Nagy, Z., Lipinszki, Z. & Sinka, R. Microtubule Organizing
510 Centers Contain Testis-Specific γ-TuRC Proteins in Spermatids of Drosophila. *Front. Cell*
511 *Dev. Biol.* **9**, 727264 (2021).
512 15. Tokuyasu, K. T. Dynamics of spermiogenesis in Drosophila melanogaster. VI. Significance
513 of 'onion' nebenkern formation. *J. Ultrastruct. Res.* **53**, 93–112 (1975).
514 16. Avasthi, P. & Marshall, W. F. Stages of ciliogenesis and regulation of ciliary length. *Differ.*
515 *Res. Biol. Divers.* **83**, S30-42 (2012).
516 17. Laurinyecz, B. *et al.* Sperm-Leucylaminopeptidases are required for male fertility as
517 structural components of mitochondrial paracrystalline material in Drosophila melanogaster
518 sperm. *PLoS Genet.* **15**, 1–24 (2019).

519 18. Chen, J. V., Buchwalter, R. A., Kao, L.-R. & Megraw, T. L. A Splice Variant of Centrosomin
520 Converts Mitochondria to Microtubule-Organizing Centers. *Curr. Biol. CB* **27**, 1928-1940.e6
521 (2017).
522 19. Vedelek, V. *et al.* Analysis of Drosophila melanogaster testis transcriptome 06 Biological
523 Sciences 0604 Genetics. *BMC Genomics* **19**, 1–19 (2018).
524 20. Wasbrough, E. R. *et al.* The Drosophila melanogaster sperm proteome-II (DmSP-II). *J.*
525 *Proteomics* **73**, 2171–2185 (2010).
526 21. Barbosa, V., Yamamoto, R. R., Henderson, D. S. & Glover, D. M. Mutation of a Drosophila
527 gamma tubulin ring complex subunit encoded by discs degenerate-4 differentially disrupts
528 centrosomal protein localization. *Genes Dev.* **14**, 3126–3139 (2000).
529 22. Colombié, N. *et al.* The Drosophila gamma-tubulin small complex subunit Dgrip84 is
530 required for structural and functional integrity of the spindle apparatus. *Mol. Biol. Cell* **17**,
531 272–282 (2006).
532 23. Vogt, N., Koch, I., Schwarz, H., Schnorrer, F. & Nüsslein-Volhard, C. The gammaTuRC
533 components Grip75 and Grip128 have an essential microtubule-anchoring function in the
534 Drosophila germline. *Dev. Camb. Engl.* **133**, 3963–3972 (2006).
535 24. Bärenz, F., Mayilo, D. & Gruss, O. J. Centriolar satellites: Busy orbits around the
536 centrosome. *Eur. J. Cell Biol.* **90**, 983–989 (2011).
537 25. Gupta, H. *et al.* SAS-6 Association with γ-Tubulin Ring Complex Is Required for Centriole
538 Duplication in Human Cells. *Curr. Biol.* **30**, 2395-2403.e4 (2020).
539 26. Fabian, L. & Brill, J. A. Big things come from little packages Drosophila spermiogenesis. 1–
540 16 (2012).

541 27. Bre, M. H. *et al.* Axonemal tubulin polyglycylation probed with two monoclonal antibodies:
542 widespread evolutionary distribution, appearance during spermatozoan maturation and
543 possible function in motility. *J. Cell Sci.* **109**, 727–738 (1996).
544 28. Noguchi, T., Koizumi, M. & Hayashi, S. Sustained elongation of sperm tail promoted by
545 local remodeling of giant mitochondria in Drosophila. *Curr. Biol.* **21**, 805–814 (2011).
546 29. Martinez-Campos, M., Basto, R., Baker, J., Kernan, M. & Raff, J. W. The Drosophila
547 pericentrin-like protein is essential for cilia/flagella function, but appears to be dispensable
548 for mitosis. *J. Cell Biol.* **165**, 673–683 (2004).
549 30. Zupa, E., Liu, P., Würtz, M., Schiebel, E. & Pfeffer, S. The structure of the γ-TuRC: a 25-
550 years-old molecular puzzle. *Curr. Opin. Struct. Biol.* **66**, 15–21 (2021).
551 31. Bourbon, H.-M. *et al.* A P-insertion screen identifying novel X-linked essential genes in
552 Drosophila. *Mech. Dev.* **110**, 71–83 (2002).
553 32. Dzhindzhev, N. S. *et al.* Asterless is a scaffold for the onset of centriole assembly. *Nature*
554 **467**, 714–718 (2010).
555 33. Allan, V. J., Thompson, H. M. & McNiven, M. A. Motoring around the Golgi. *Nat. Cell Biol.*
556 **4**, E236–E242 (2002).
557 34. Kondylis, V. & Rabouille, C. The Golgi apparatus: Lessons from Drosophila. *FEBS Lett.*
558 **583**, 3827–3838 (2009).
559 35. Gillingham, A. K., Sinka, R., Torres, I. L., Lilley, K. S. & Munro, S. Toward a
560 Comprehensive Map of the Effectors of Rab GTPases. *Dev. Cell* **31**, 358 (2014).
561 36. Morohoshi, A. *et al.* FAM71F1 binds to RAB2A and RAB2B and is essential for acrosome
562 formation and male fertility in mice. *Development* **148**, dev199644 (2021).

563 37. Riparbelli, M. G., Persico, V. & Callaini, G. The Microtubule Cytoskeleton during the Early
564 Drosophila Spermiogenesis. *Cells* **9**, 1–18 (2020).
565 38. Fu, J. *et al.* Conserved molecular interactions in centriole-to-centrosome conversion. *Nat.*
566 *Cell Biol.* **18**, 87–99 (2016).
567 39. Gopalakrishnan, J. *et al.* Tubulin nucleotide status controls Sas-4-dependent pericentriolar
568 material recruitment. *Nat. Cell Biol.* **14**, 865–873 (2012).
569 40. Galletta, B. J. *et al.* A centrosome interactome provides insight into organelle assembly and
570 reveals a non-duplication role for Plk4. *Nat. Commun.* **7**, 12476 (2016).
571 41. Gopalakrishnan, J. *et al.* Sas-4 provides a scaffold for cytoplasmic complexes and tethers
572 them in a centrosome. *Nat. Commun.* **2**, 359 (2011).
573 42. Guruharsha, K. G. *et al.* A Protein Complex Network of Drosophila melanogaster. *Cell* **147**,
574 690–703 (2011).
575 43. Dzhindzhev, N. S. *et al.* Plk4 phosphorylates Ana2 to trigger Sas6 recruitment and
576 procentriole formation. *Curr. Biol. CB* **24**, 2526–2532 (2014).
577 44. Moritz, M., Zheng, Y., Alberts, B. M. & Oegema, K. Recruitment of the gamma-tubulin ring
578 complex to Drosophila salt-stripped centrosome scaffolds. *J. Cell Biol.* **142**, 775–786
579 (1998).
580 45. Kurucz, E. *et al.* Assembly of the Drosophila 26 S proteasome is accompanied by
581 extensive subunit rearrangements. *Biochem. J.* **365**, 527 (2002).
582 46. Efimov, A. *et al.* Asymmetric CLASP-dependent nucleation of non-centrosomal
583 microtubules at the trans-Golgi network. *Dev. Cell* **12**, 917–930 (2007).
584 47. Becker, R. *et al.* Myogenin controls via AKAP6 non-centrosomal microtubule-organizing
585 center formation at the nuclear envelope. *eLife* **10**, e65672 (2021).

586 48. Brodu, V., Baffet, A. D., Le Droguen, P.-M., Casanova, J. & Guichet, A. A developmentally
587 regulated two-step process generates a noncentrosomal microtubule network in Drosophila
588 tracheal cells. *Dev. Cell* **18**, 790–801 (2010).
589 49. Tovey, C. A. *et al.* Autoinhibition of Cnn binding to γ-TuRCs prevents ectopic microtubule
590 nucleation and cell division defects. *J. Cell Biol.* **220**, e202010020 (2021).
591 50. Mukherjee, A., Brooks, P. S., Bernard, F., Guichet, A. & Conduit, P. T. Microtubules
592 originate asymmetrically at the somatic golgi and are guided via Kinesin2 to maintain
593 polarity within neurons. *eLife* **9**, e58943 (2020).
594 51. Rivero, S., Cardenas, J., Bornens, M. & Rios, R. M. Microtubule nucleation at the cis-side
595 of the Golgi apparatus requires AKAP450 and GM130. *EMBO J.* **28**, 1016–1028 (2009).
596 52. Lund, V. K., Madsen, K. L. & Kjaerulff, O. Drosophila Rab2 controls endosome-lysosome
597 fusion and LAMP delivery to late endosomes. *Autophagy* **14**, 1520–1542 (2018).
598 53. Fári, K., Takács, S., Ungár, D. & Sinka, R. The role of acroblast formation during
599 *Drosophila* spermatogenesis. *Biol. Open* **5**, 1102–1110 (2016).
600 54. Chen, D. & McKearin, D. M. A discrete transcriptional silencer in the bam gene determines
601 asymmetric division of the Drosophila germline stem cell. *Dev. Camb. Engl.* **130**, 1159–
602 1170 (2003).
603 55. Gibson, D. G. *et al.* Enzymatic assembly of DNA molecules up to several hundred
604 kilobases. *Nat. Methods* **6**, 343–345 (2009).
605 56. Port, F. & Bullock, S. L. Creating Heritable Mutations in Drosophila with CRISPR-Cas9. in
606 *Methods in Molecular Biology* vol. 1478 145–160 (2016).

607 57. Port, F., Chen, H. M., Lee, T. & Bullock, S. L. Optimized CRISPR/Cas tools for efficient
608 germline and somatic genome engineering in Drosophila. *Proc. Natl. Acad. Sci. U. S. A.*
609 **111**, (2014).
610 58. Alzyoud, E., Vedelek, V., Réthi-Nagy, Z., Lipinszki, Z. & Sinka, R. Microtubule Organizing
611 Centers Contain Testis-Specific γ-TuRC Proteins in Spermatids of Drosophila. *Front. Cell*
612 *Dev. Biol.* **9**, (2021).
613 59. White-cooper, H. Analysis of Meiosis and Morphogenesis. *Drosoph. Cytogenet. Protoc.*
614 **247**, 468 (2004).
615 60. James, P., Halladay, J. & Craig, E. A. Genomic Libraries and a Host Strain Designed for
616 Highly Efficient Two-Hybrid Selection in Yeast. *Genetics* **144**, 1425–1436 (1996).
617 61. Karman, Z. *et al.* Novel perspectives of target-binding by the evolutionarily conserved PP4
618 phosphatase. *Open Biol.* **10**, 200343 (2020).
619 62. Réthi-Nagy, Z., Ábrahám, E. & Lipinszki, Z. GST-IVTT pull-down: a fast and versatile
620 in vitro method for validating and mapping protein-protein interactions. *FEBS Open Bio* **12**,
621 1988–1995 (2022).
622 63. Jones, R. B. *et al.* Golgi coiled-coil proteins contain multiple binding sites for rab family G
623 proteins. *J. Cell Biol.* **183**, 607–615 (2008).
624
625

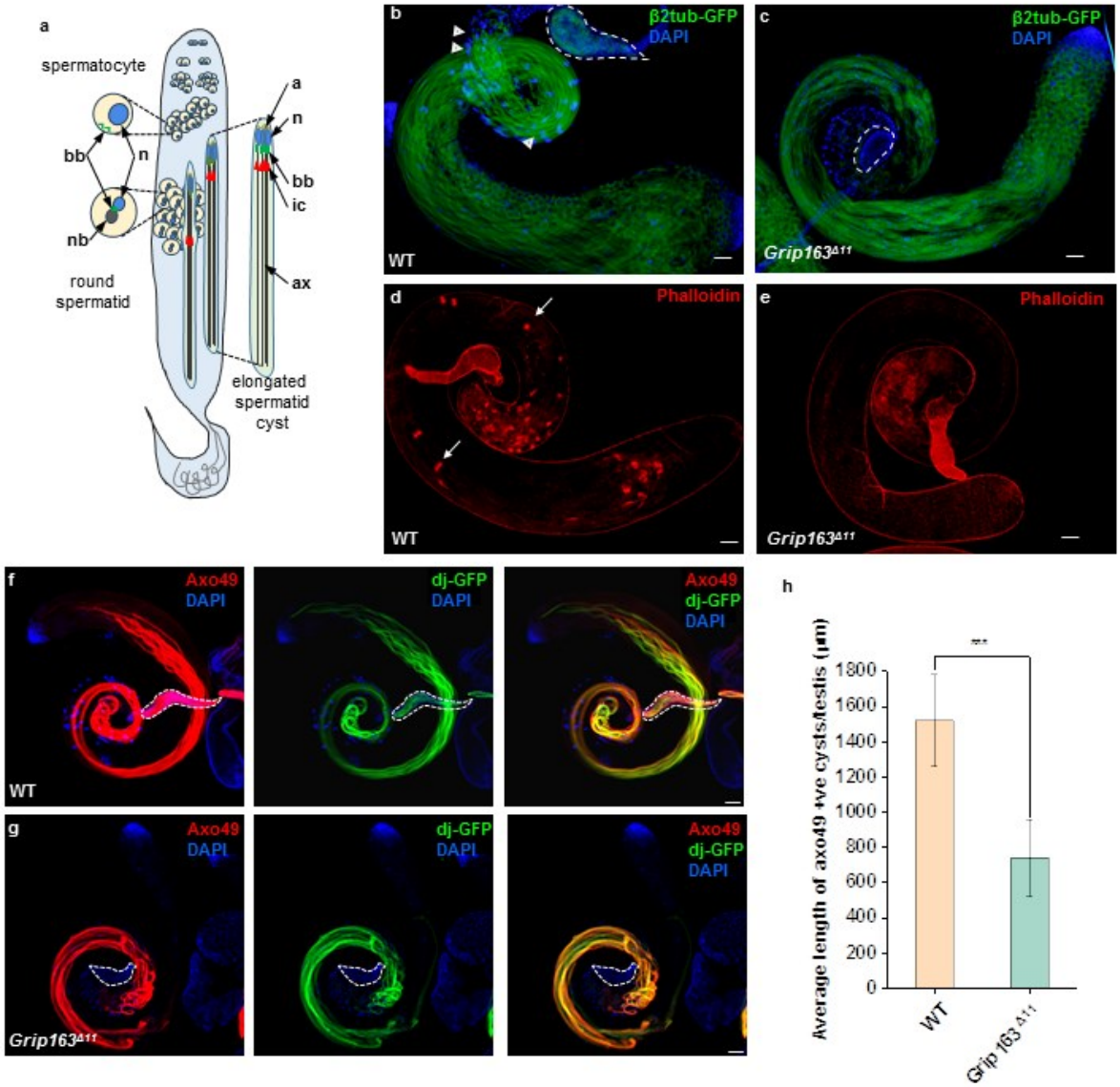

Figure 1. Mitochondrial and axonemal abnormalities lead to abnormal spermatid elongation in *Grip163$^{\Delta 11}$* mutant

(**a**) Schematic representation of Drosophila spermatogenesis stages in the testis, highlighting the major cellular organelles (bb: basal body, n: nucleus, nb: nebenkern, a: acrosome, ax: axoneme and cytoskeletal structures (ic: investment cone) of the secondary spermatocyte, round spermatids and the elongated spermatid cyst. **(b, c)** Microtubules are visualized with the β2tub-GFP transgene (green), while the nuclei stained with DAPI (blue) in WT **(b)** and *Grip163$^{\Delta 11}$* mutant spermatids **(c)** Elongated cysts are present both in WT and *Grip163$^{\Delta 11}$*, however, the seminal vesicle (dashed lines) of *Grip163$^{\Delta 11}$* mutant does not contain β2tub-GFP positive mature sperms. **(d,e)** The individualization complexes (IC) were stained with Phalloidin (red), ICs are formed normally (arrows) in WT, **(c)** and missing in *Grip163$^{\Delta 11}$* mutant **(e)**. **(f, g)** Fully developed axonemes are visualized by Axo49 tubulin antibody (red) and elongated mitochondria

are with DJ-GFP transgene (green) both in the testis and seminal vesicle (dashed line). Elongated polyglycylated axonemes and mitochondria were shorter in *Grip163*$^{\Delta 11}$ mutant and the seminal vesicle was empty (dashed line) **(g)** compared to the WT **(f). (h)** Diagrams show the average length of Axo49 positive cysts in WT and *Grip163*$^{\Delta 11}$ mutant. (WT n=12, *Grip163*$^{\Delta 11}$ n=22) Statistical significance was tested by one-way ANOVA. (scale bars: 50 µm).

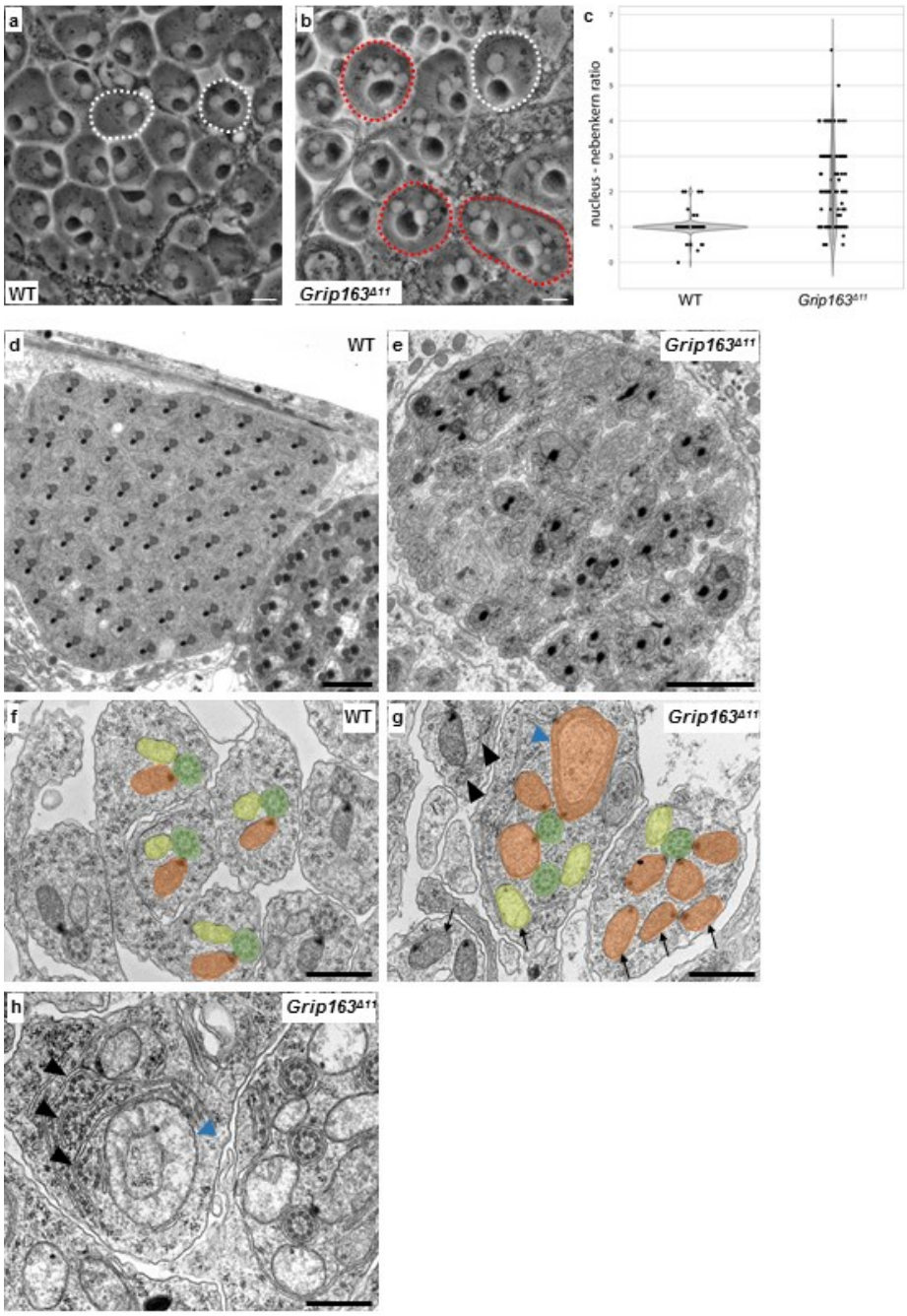

Figure 2: Abnormal mitochondrial and axonemal structures in the post-meiotic cysts of *Grip163*$^{\Delta 11}$ mutant

(a, b) Phase contrast images show a normal 1:1 (white outline), nucleus: nebenkern ratio in WT **(a)** and an abnormal ratio (red outline) in *Grip163*$^{\Delta 11}$ mutant **(b)**. **(c)** Violin plot showing the nucleus: nebenkern ratio in WT (n=186) and *Grip163*$^{\Delta 11}$ mutant round spermatids (n=112). **(d, h)** Transmission electron micrograms of testis cross-sections, representing elongating cysts of WT (**d,f**) and *Grip163*$^{\Delta 11}$ mutant (**e,g,h**). Disorganized cysts with axonemal and mitochondrial abnormalities are characteristic in *Grip163*$^{\Delta 11}$ mutant**. (f)** WT elongating cyst shows normal axoneme structure with 9+2 tubulin dimers (highlighted in green) and two mitochondrial derivatives (yellow and orange), with paracrystalline material formation in one of them (orange). **(g, h)** In *Grip163*$^{\Delta 11}$ mutant the mitochondria and the axoneme detached from each other, and multiple mitochondrial derivatives (highlighted in orange and yellow) attached to one axoneme (green). **(h)** Mitochondria fused, enlarged (blue arrowheads) and detached (arrow) from the axoneme and disintegrated axonemes with microtubule bundles and the axial membrane opening is characteristic of *Grip163*$^{\Delta 11}$ mutant cyst (black arrowheads). (scale bars: A-E 2 µm, F-H 500 nm)

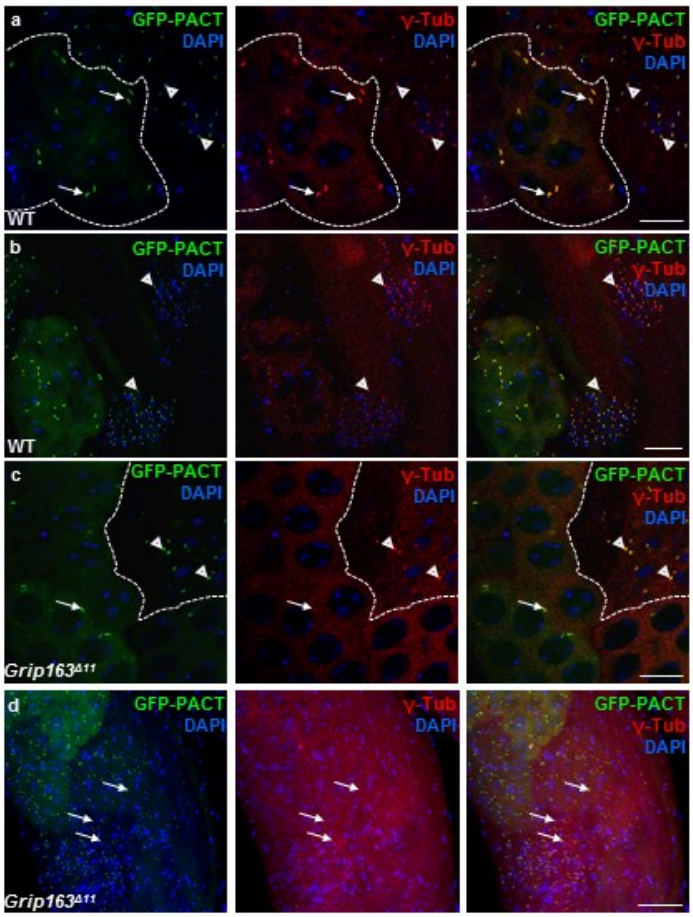

Figure 3: Mislocalization of centrosomal markers in *Grip163*$^{\Delta 11}$mutant

(a-b) GFP-PACT (green) and γ-Tubulin (red) are colocalizing on the centrosome (arrows) and basal body (arrowheads) in WT spermatocytes and spermatids **(a, b)**. γ-tubulin, but not GFP-PACT centrosomal localization is affected in *Grip163*$^{\Delta 11}$ mutant spermatocytes. In the round spermatids, GFP-PACT and γ-Tubulin are colocalised **(c)**, but the post-meiotic elongating cysts are disorganized with scattered basal bodies. **(d)**. (scale bars: 20 µm)

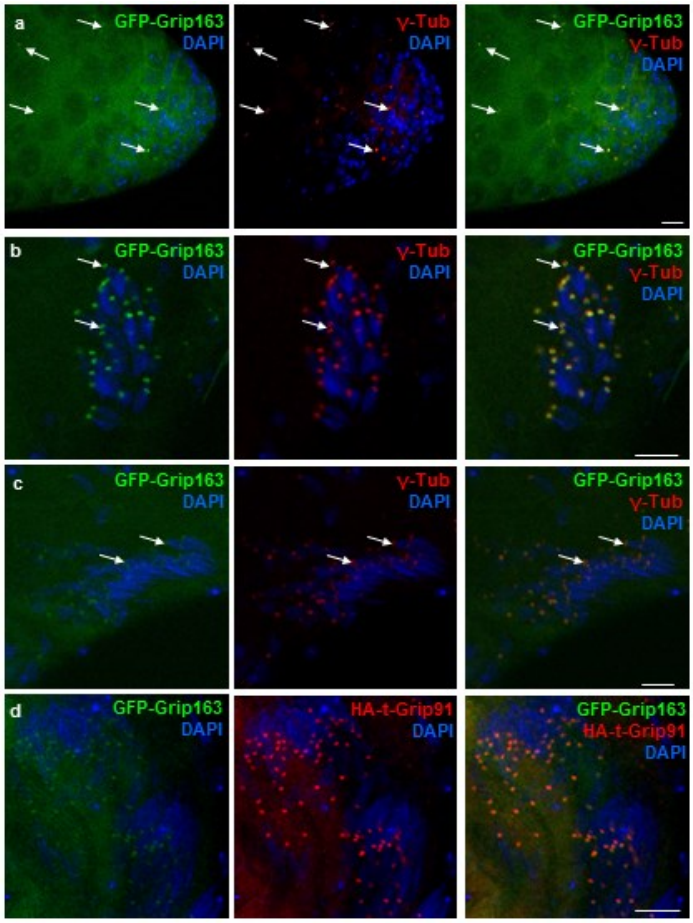

Figure 4: Localization of GFP-Grip163 during spermatogenesis.
(a-c) The endogenously tagged GFP-Grip163 colocalizes with γ-Tubulin at the **(a)** centrosome (arrows) and the **(b-c)** basal body (arrows) throughout spermatogenesis. **(d)** GFP-Grip163 has an overlapping localization with the t-γ-TuRC represented by HA-t-Grip91 on the basal body/centriole adjunct in the elongating spermatids**)**. (scale bars: 10 µm)

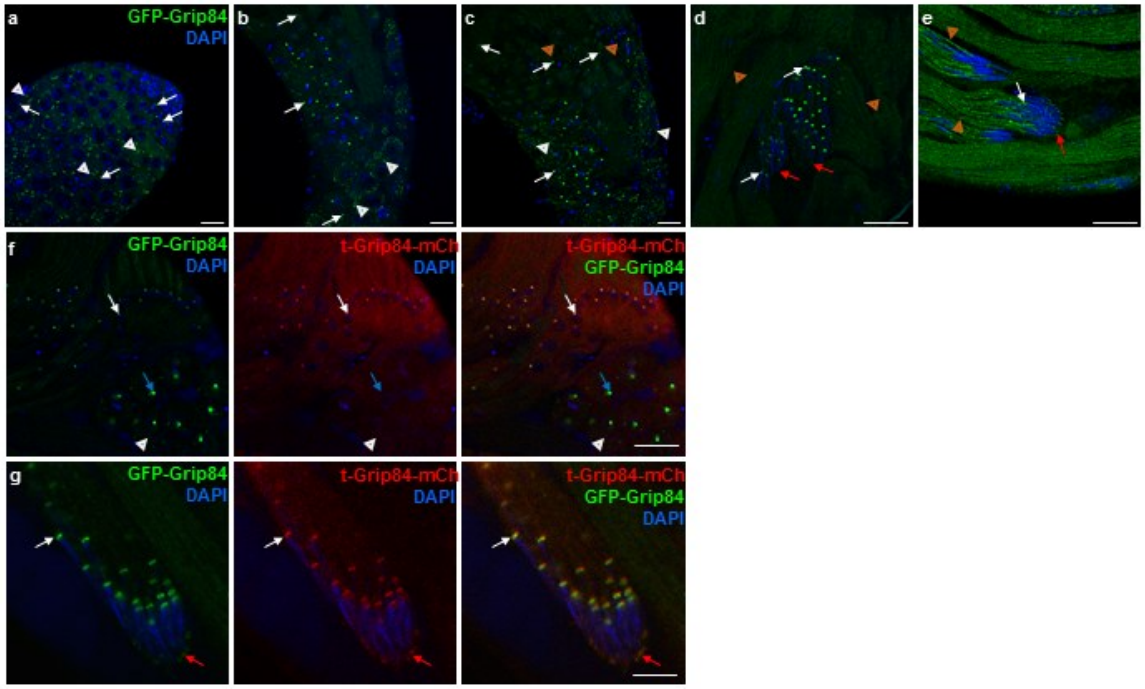

Figure 5: Localization of GFP-Grip84 during spermatogenesis.
(a-e) *In vivo* tagged GFP-Grip84 localizes both to the centrosome (**a**) and the basal body (**b**, **c**) (white arrows) and in the post-meiotic elongating cyst GFP-Grip84 localizes also to the apical tip of the elongating nuclei (**d, e**) (red arrows). Additionally, it is localized surrounding the elongating mitochondria (**c-e**) (orange arrowheads). Golgi-like localization of GFP-Grip84 was observed in spermatocytes (**c**) (white arrowheads). **(f, g)** GFP-Grip84 localizes to the centrosome before meiosis (blue arrows) and shows overlapping localization with t-Grip84-mCh at the basal body (white arrows) and the apical tip of the elongating nuclei (red arrows) in the post-meiotic spermatids (Scale bars: 20 μm).

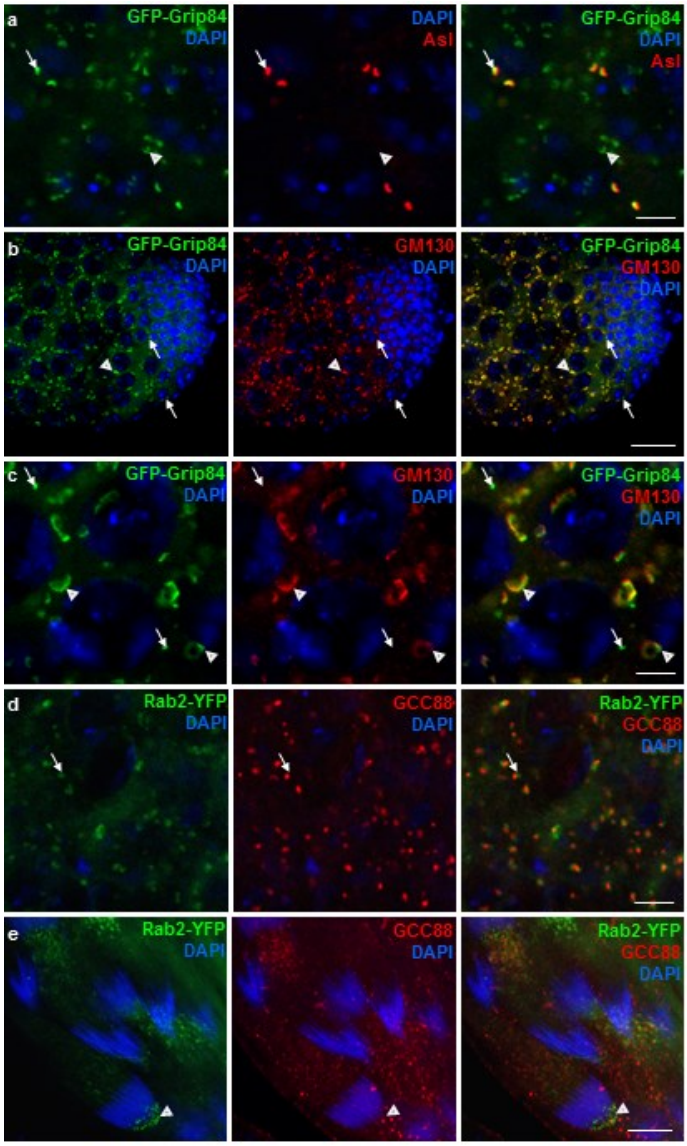

Figure 6: γ-TuSC protein GFP-Grip84 is localizing to the Golgi in spermatocytes

(a) GFP-Grip84 colocalizes with centrosomal protein Asl (anti-Asl, white arrow) and also to the Golgi apparatus (white arrowhead). **(b, c)** GFP-Grip84 colocalizes with antibody-stained *cis*-Golgi marker GM130 in the spermatocytes (arrowheads). **(d, e)** Rab2-YFP localizes to the Golgi (arrow) in spermatocytes visualised by the *trans*-Golgi marker GCC88 and also to the apical end of the elongating nuclei (arrowhead). (Scale bars: A, C, D 10 µm, B, E20 µm).

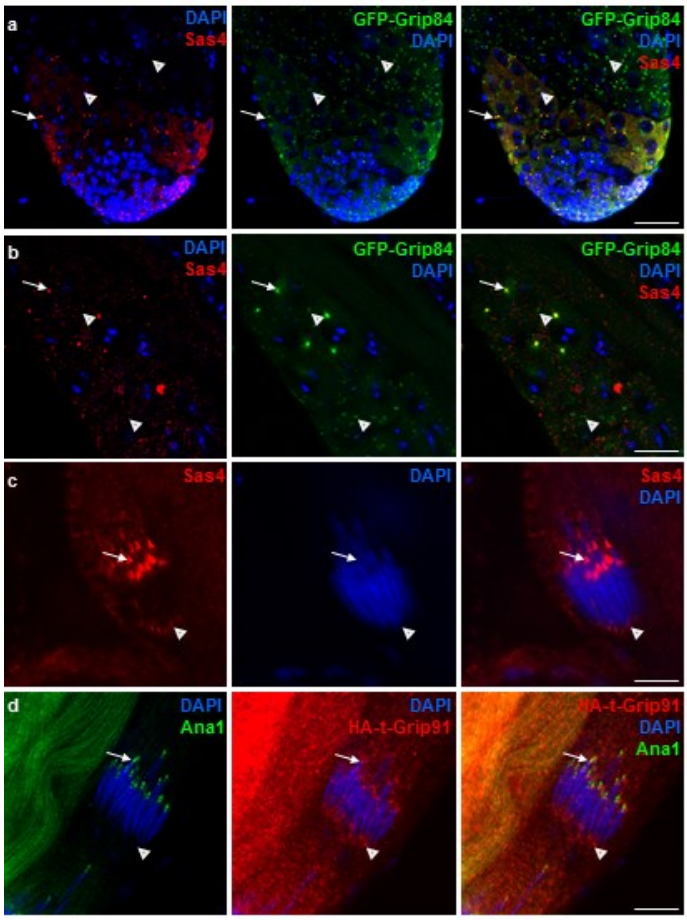

Figure 7: Sas4 is a component of the site, which has been suggested as a ncMTOC at the apical tip of the elongating nuclei

(a, b) Antibody-stained Sas4 (red) colocalizes with the endogenous tag GFP-Grip84 at the centrosome (arrows) but not on the Golgi (arrowheads) in the spermatocytes. **(c)** Sas4 (red) is localizing to the basal body of the elongating spermatids (arrows) and additionally to the apical tip of the nuclei (arrowheads). **(d)** Antibody-stained Ana1 localizes only to the basal body (arrows) of the elongating spermatids, while the t-γ-TuRC component HA-t-Grip91 localizes to the basal body(arrow) and the apical tip (arrowheads) of the elongating spermatids. (Scale bars: 20 µm).

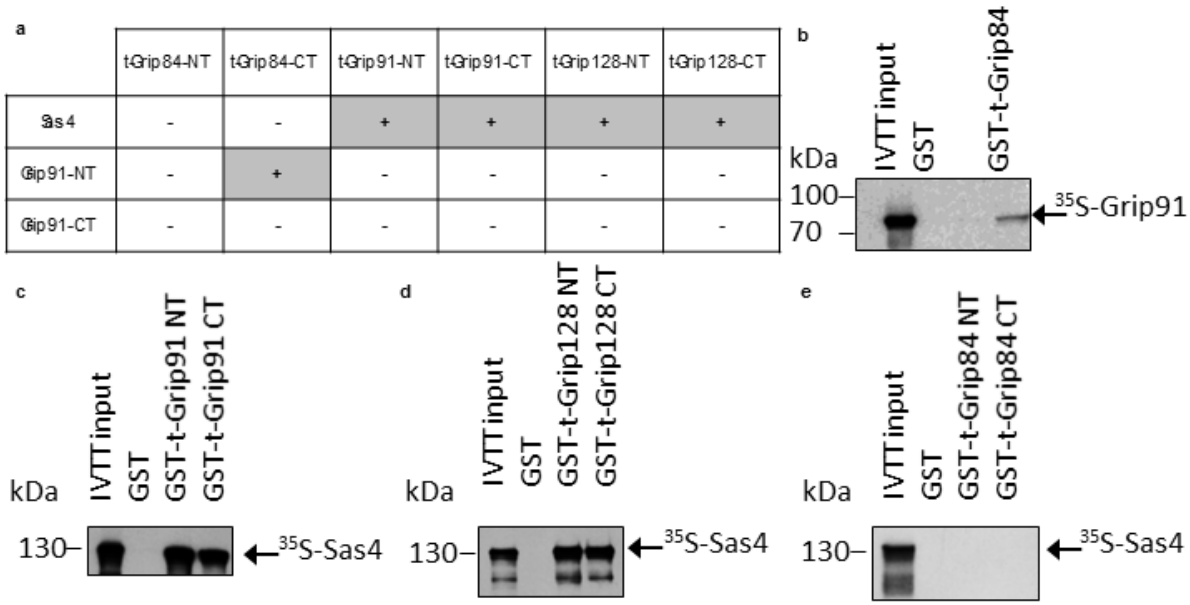

Figure 8: Interactions of t-γ-TuRC proteins with Sas4 and the canonical Grip91.
(a) Summary of Y2H analysis of the N- or C-terminal parts of t-γ-TuRC proteins (as indicated in the table) with Sas4, and the N- or C-terminal parts of Grip91, respectively. **(b-e)** Autoradiographic images show the presence or absence of interaction between purified and immobilised GST-t-γ-TuRC protein fragments and ^{35}S-labelled Sas4 or Grip91, synthesized by *in vitro* transcription-translation (IVTT) reaction.

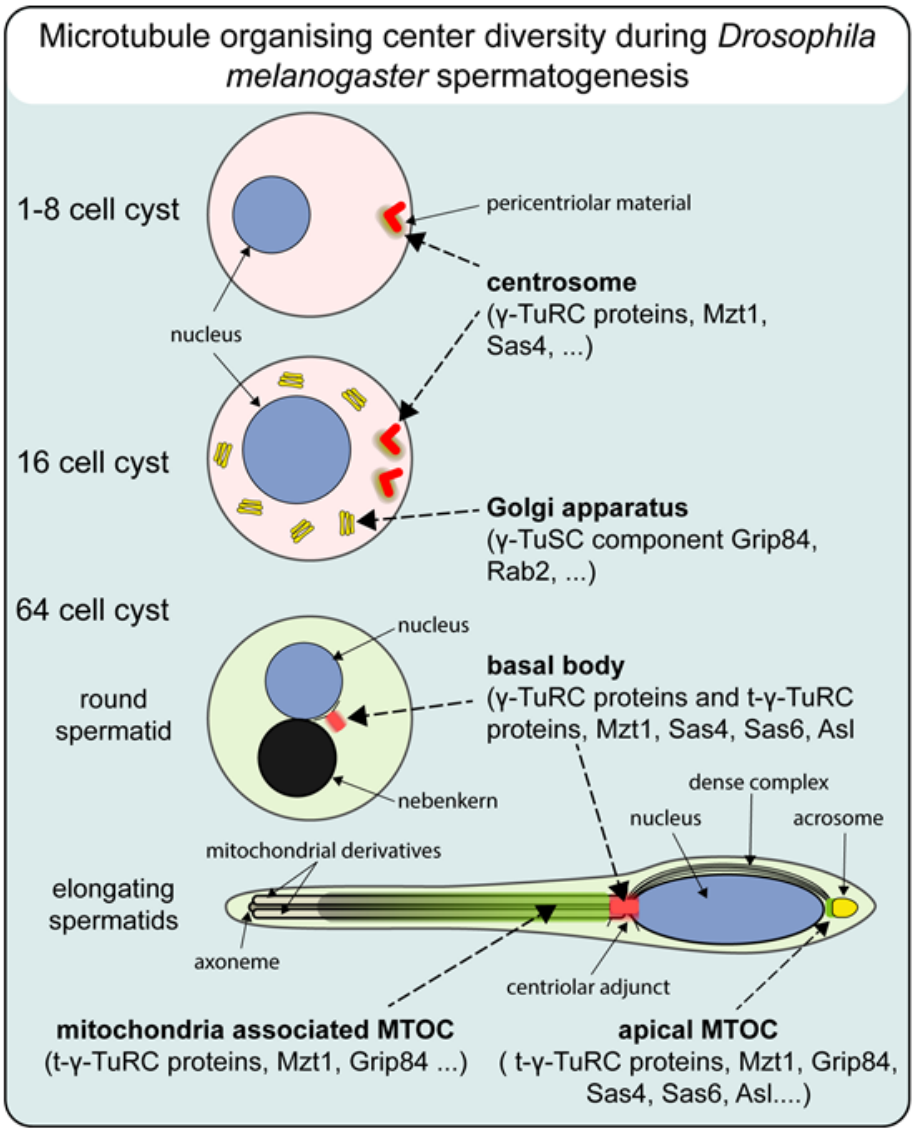

Figure 9: Summary of localization of γ-TuRC/t-γ-TuRC containing MTOCs during different stages of spermatogenesis

715 **Supplementary Table1 List of antibodies used in immunostaining.**

Antibody /Dye	Dilution	Source	Identifier	Fixation method
anti-HA (rat)	1:100	Sigma-Aldrich/Roche	Cat# 11867423001	Formaldehyde
anti-Sas4 (rat)	1:500	[38]		Methanol-acetone
anti-Sas6 (rat)	1:500	[43]		Methanol-acetone
GM130 (rabbit)	1:500	Abcam	ab30637	Formaldehyde
GCC88 (G. pig)	1:100	[63]		Formaldehyde
Anti-GFP (rabbit)	1:500	Thermo Fisher Scientific	Cat#A-11122	Methanol-acetone
anti-pan polyglycylated Tubulin Axo49 (mouse)	1:5000	Sigma-Aldrich/Merck	Cat# MABS276	Formaldehyde
anti-γ-Tubulin (mouse)	1:5000	Sigma-Aldrich/Merck	Cat# T6557	Formaldehyde
anti-Ana1 (rabbit)	1:5000	[38]	-	Formaldehyde
anti-Asl (rabbit)	1:1000	[32]	-	Methanol-acetone
G.pig Alexa Fluor 546 secondary	1:400	ThermoFisher	Cat# A-11074	
Mouse Alexa Fluor 488 secondary	1:400	Thermo Fisher Scientific	Cat#A-11029	
Mouse Alexa Fluor 546 secondary	1:400	Thermo Fisher Scientific	Cat#A-11030	
Mouse Alexa Fluor 633 secondary	1:400	Thermo Fisher Scientific	Cat#A-21052	
Rat Alexa Fluor 488 secondary	1:400	Thermo Fisher Scientific	Cat#A-21208	
Rat Alexa Fluor 568 secondary	1:400	Thermo Fisher Scientific	Cat#A-11081	

Rabbit Alexa Fluor 488 secondary	1:400	Thermo Fisher Scientific	Cat#A-11008	
Rabbit Alexa Fluor 546 secondary	1:400	Thermo Fisher Scientific	Cat#A-11010	
4',6-Diamidino-2-Phenylindole, Dihydrochloride (DAPI)	1 µg/ml	Thermo Fisher Scientific	Cat#D1306	

716

717 **Supplementary Table2 List of oligonucleotide primers uses in this study**

Primer Name	Primer Sequence
Grip163-gRNA-fwd	tgcagtgcttctccggtccaggct
Grip163-gRNA-rev	aaacagcctggaccggagaagcac
Grip163-1.5 kb upstream_fwd	gtgccacctgacgtctaagagatacatcccataattaccatacttacccag
Grip163-1.5 kb upstream_rev	tgctcaccatcaggggtttcagggcgcg
Grip163-GFP_fwd	gaaacccctgatggtgagcaagggcgag
Grip163-GFP_rev	gctgtagttgcttgtacagctcgtccatg
Grip163-before PAM_fwd	gctgtacaagcaactacagccatactccg
Grip163-before PAM_rev	ccaggctgtgccacaaaaggtcgttcatc
Grip163-Mutant PAM_fwd	ccttttgtggcacagcctggaccggagaag
Grip163-Mutant PAM_rev	gagttagctcactcattaggggtcaggactggacgacag
pJET1_fwd	cctaatgagtgagctaactcac
pJET1_rev	tcttagacgtcaggtggcac
Grip84-gRNA-fwd	tgcaatccttgagcggctaccgct
Grip84-gRNA-rev	aaacagcggtagccgctcaaggat
Grip84-1.5 kb upstream-fwd	ccacctgacgtctaagatgacccgctgaccatggc
Grip84-1.5 kb upstream-rev	ctcaccattacgggtgtagtgtcggattc
Grip84-GFP_fwd	cacccgtaatggtgagcaagggcgag
Grip84-GFP_rev	acaaagaccttgtacagctcgtccatg
Grip84-before PAM_fwd	gctgtacaaggtctttgtcaggcgcggc
Grip84-before PAM _rev	acagagcggtagccgctcaaggattg
Grip84-mutant PAM_fwd	cggctaccgctctgtgaccaacaaaacg
Grip84-mutant PAM_rev	ttagctcactcattagggctcgcagtgcagatcgtc
YTH Sas4_fwd	atcgccggaattcccaatgcaggaggctggcgaaag
YTH Sas4_rev	ggtcgacggatccccctaatacttggcatagtctgtgtccattatg
YTH Grip91-N_fw	atcgccggaattcccaATGTCGCAGGACAGGATCGC
YTH Grip91-N_rev	ggtcgacggatcccctta CCCCACCATAATGTCGAGGAC
YTH Grip91-C_fw	atcgccggaattccca
YTH Grip91-C_rev	ggtcgacggatccccttа

YTH Grip84_fw	atcgccggaattccca
YTH Grip84_rev	ggtcgacggatcccctta
YTH Grip75_fw	atcgccggaattccca
YTH Grip75_rev	ggtcgacggatccccctaa
YTH Grip128-N_fw	atcgccggaattccca
YTH Grip128-N_rev	ggtcgacggatccccctaa
YTH Grip128-C_fw	atcgccggaattccca
YTH Grip128-C_rev	ggtcgacggatccccctaa
YTH Grip163-N_fw	atcgccggaattccca
YTH Grip163-N_rev	ggtcgacggatccccctaa
YTH Grip163-C_fw	atcgccggaattccca
YTH Grip163-C_rev	ggtcgacggatccccctaa
GST t-Grip91-N_fw	cgacggtaccatggagacgcagccatttaaaat
GST t-Grip91-N_rev	gcggccgcttaaactaacatagggtatcaatttcaac
GST t-Grip128-N_fw	cgacggtaccatgcaagaggacgagagaca
GST t-Grip128-N_rev	gcggccgcttatcgttcatcggtcacaatc
GST t-Grip128-C_fw	cgacggtaccatgacagagtacgtcttaagaaaatc
GST t-Grip128-C_rev	gcggccgcttaaatatggccgagcaaaca
GST t-Grip84-N_fw	gaattcaaatgaactccgacaaatcggaaagtg
GST t-Grip84-N_rev	gcggccgcttaattgtgctcctccacc
GST t-Grip84-C_fw	gaattcaaatgttgcctttacacattcg
GST t-Grip84-C_rev	gcggccgcttaaatattggaagctatttgatcc

Supplementary figure 1

a

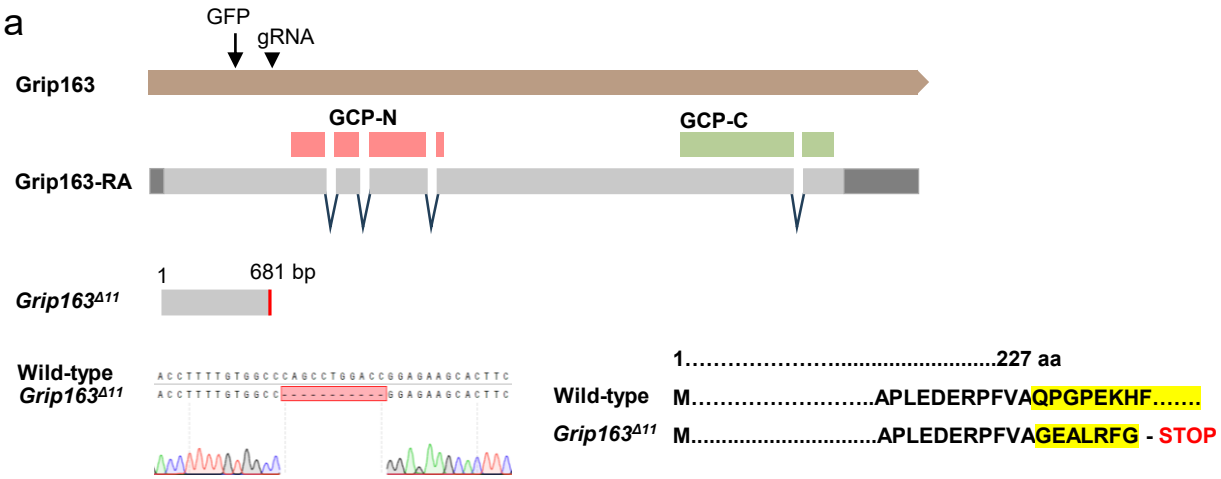

b

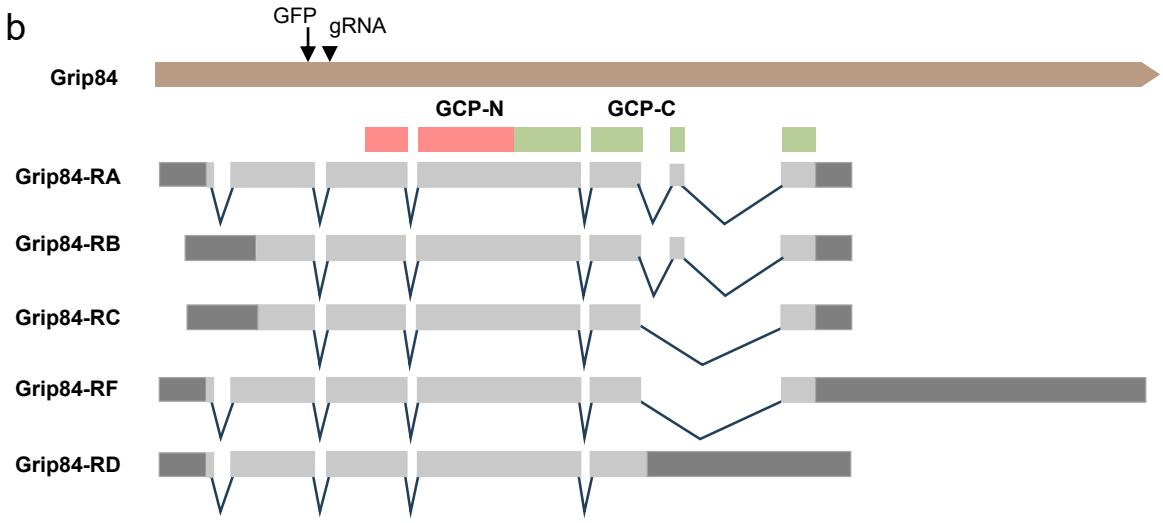

c

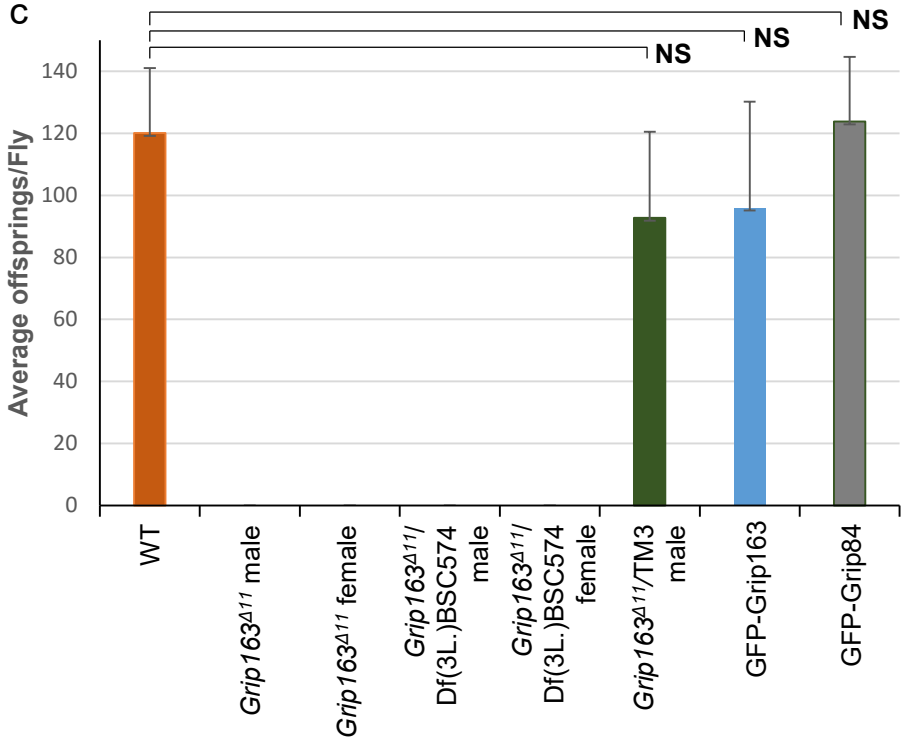

Supplementary Figure 1: Structural arrangement of *Grip163* and *Grip84* genes and transcripts.
(a) Gene structure, transcript composition and protein domains (GCP-N, GCP-C) of Grip163. gRNA position (11,997,349..11,997,371 [+]) and the position of the *in vivo* inserted GFP tag (11,997,601 [-]) is labelled. *Grip163*$^{\Delta 11}$ mutant has an 11bp deletion (11,997,369..11,997,359). The DNA and the protein sequences surrounding the deletion are shown. **(b)** Gene structure of Grip84 with the sites of gRNA (19,564,635..19,564,657 [-]) and the GFP tag (19,564,845 [-]). The inserted GFP tag labels all five Grip84 isoforms **(c)** Graph represents the fertility test of WT (n=14), *Grip163*$^{\Delta 11}$ (n=6), *Grip163*$^{\Delta 11}$*/Cyo* (n= 12), GFP-Grip84 (n=12) and GFP-Grip163 (n=15) males. Statistical significance was tested by one-way ANOVA.

Supplementary figure 2

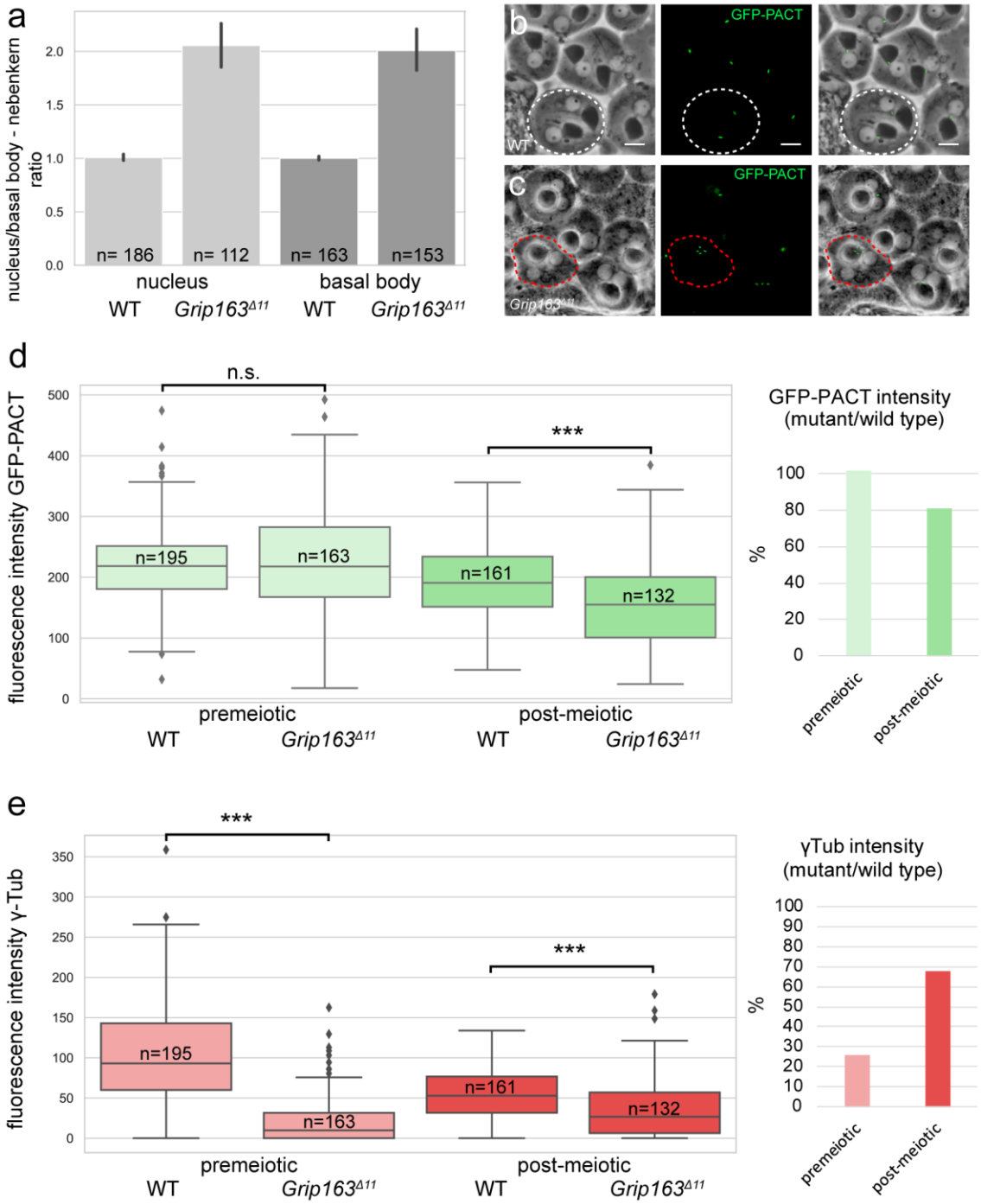

Supplementary Figure 2:Measurment of distribution of GFP-PACT and γ-Tubulin. (a) Barplot represents the mean values of nucleus/nebenkern and basal body/nebenkern ratios in round spermatids. Error bars show 95% confidence intervals. The number of spermatid cyst fragments is indicated at the base of the columns (each category is represented ~300 round spermatids). (b, c) Phase contrast images and fluorescent images of GFP-PACT (green) show wild type (b, white dashed line) and Grip163Δ11 mutant round spermatids (c, red dashed line) scale bars represent 10 µm. (d) Boxplot represents fluorescence intensity of GFP-PACT in premeiotic and post-meiotic stages of WT and Grip163Δ11. The number of measurements is indicated on the figure. Barplot indicate the ratio of fluorescence intensity in percentage between the Grip163Δ11 mutant and wild type. (e) Boxplot represents fluorescence intensity of γ-Tub in premeiotic, post-meiotic stages of wild type and Grip163Δ11. The number of measurements is indicated in the figure. The barplot indicates the ratio of fluorescence intensity in percentage between the Grip163Δ11 mutant and wild type.

Supplementary figure 3

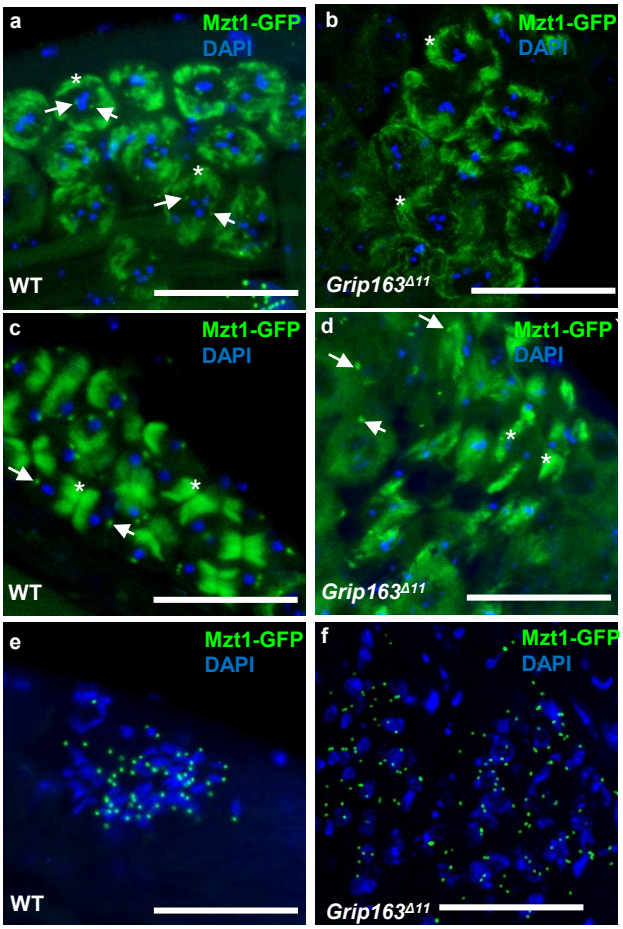

Supplementary Figure 3: Mzt1-GFP localization in WT and Grip163Δ11 mutant. (a-d) Mzt1-GFP localizes to the basal body (arrow) and mitochondria (asterisk) in WT and to the mitochondria in Grip163Δ11 mutant in dividing meiotic cysts. (e-f) Basal body localization of Mzt1-GFP is present in both in WT and Grip163Δ11 mutant.

Supplementary figure 4

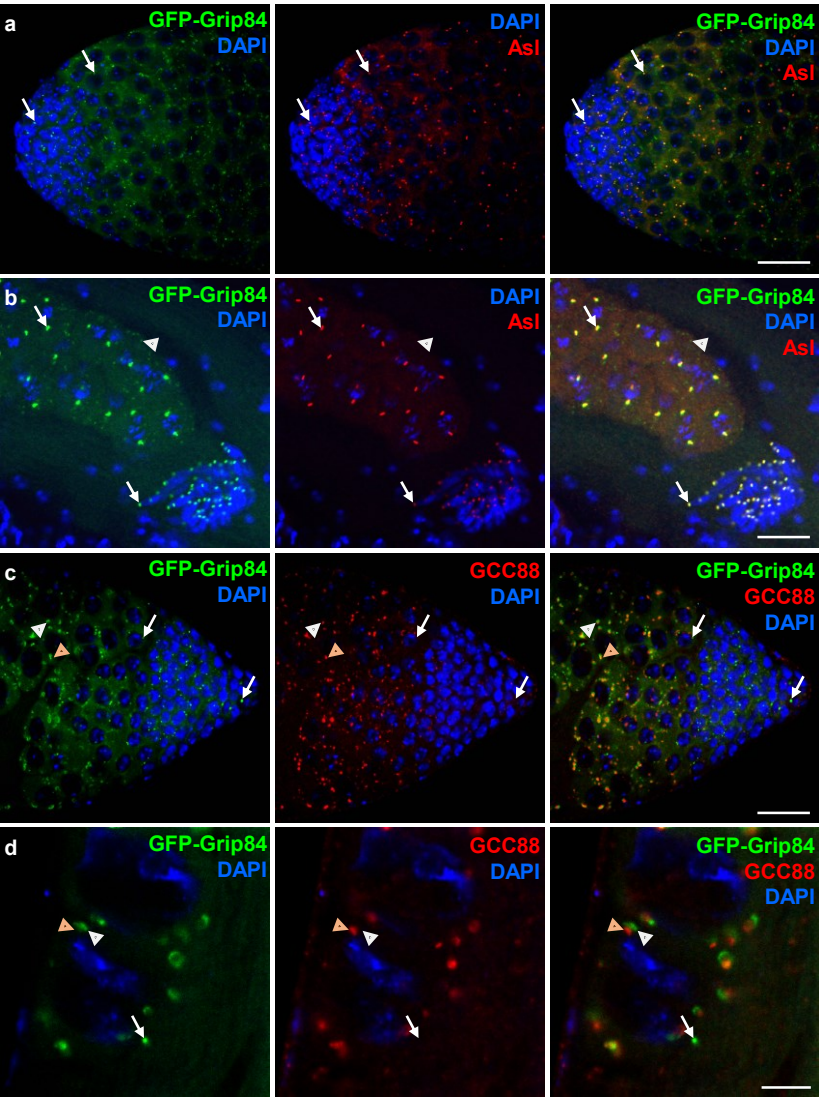

Supplementary Figure 4: Grip84 localization during spermatogenesis. (a-d) The endogenous tag GFP-Grip84 colocalizes with antibody-stained Asl (red) at the (a) centrosome (arrow) and the (b) basal body (arrow) of the spermatocytes and the spermatids, but not with the Golgi localized GFP-Grip84 (arrowhead). (c, d) GFP-Grip84 localizes adjacent to antibody-stained trans-Golgi marker GCC88 (arrowheads) and to the centrosome (arrow) in spermatocytes. (Scale bars: 20 µm).

Supplementary figure 5

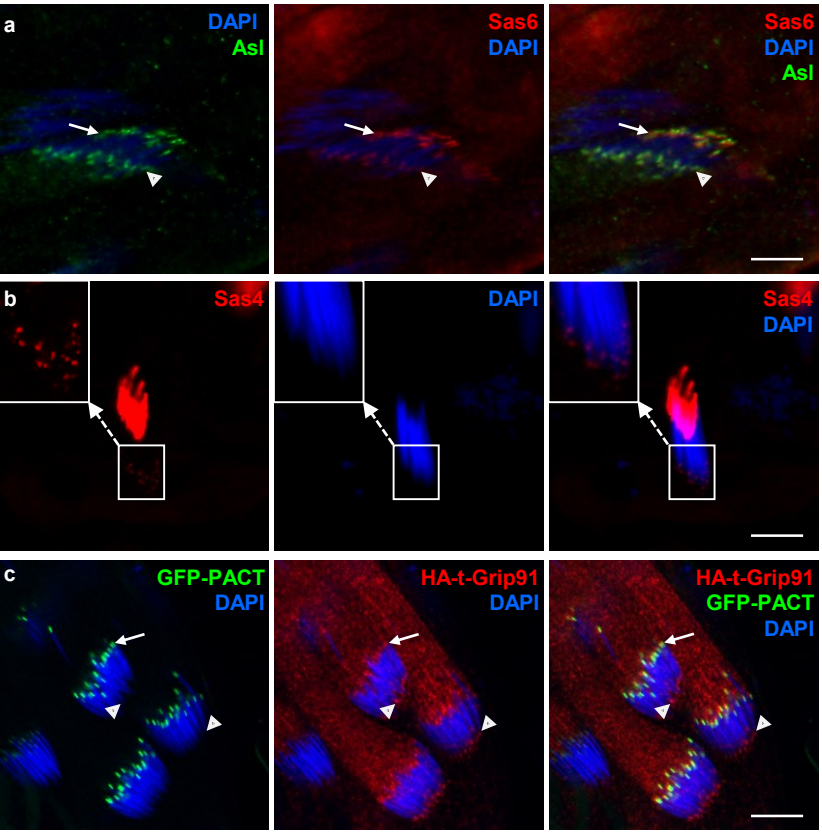

Supplementary Figure 5: Localization of centrosomal and basal body component proteins in spermatids. **(a, b)** Asl, Sas6 and Sas4 localization to the basal body (arrow) and the apical tip (arrowhead) of elongating spermatids are visualised by immunostaining using gene-specific antibodies. **(c)** GFP-PACT localizes to the basal body (arrows) of the elongating spermatids, while the HA-t-Grip91 localizes to the basal body (arrow) and the apical tip (arrowheads) of the elongating spermatids. (Scale bars: 20 µm)

Supplementary figure 6

a

Y2H fragments	
t-Grip84 NT.	1-399 aa.
t-Grip84 CT.	400-728 aa.
t-Grip91 NT.	1-966 aa.
t-Grip91 CT.	967-1932 aa.
t-Grip128 NT.	1-550 aa.
t-Grip128 CT.	551-975 aa.
Grip84	1-834 aa.
Grip91 NT.	1-544 aa.
Grip91 CT.	545-918 aa.
Grip128 NT.	1-584 aa.
Grip128 CT.	585-1093 aa.
Grip163 NT.	1-676 aa.
Grip163 CT.	677-1352 aa.
Grip75	1-650 aa.

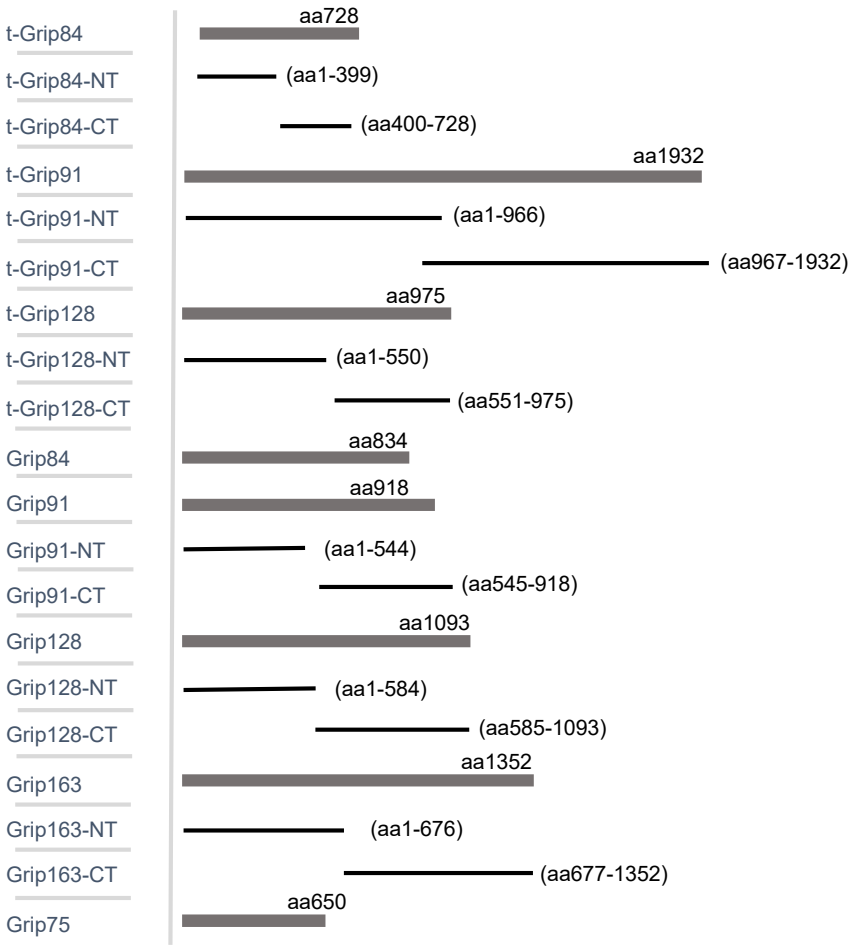

b

	t-Grip84-NT (1-399 aa)	t-Grip84-CT (400-728 aa)	t-Grip91-NT (1-966 aa)	t-Grip91-CT (967-1932 aa)	t-Grip128-NT (1-550 aa)	t-Grip128-CT (551-975 aa)
Sas4 (1-901aa)	-	-	+	+	+	+
Grip91-NT (1-545 aa)	-	+	-	-	-	-
Grip91-CT (546-917aa)	-	-	+	+	-	-
Grip84 (1-833 aa)	-	+	+	+	-	-
Grip75 (1-650 aa)	-	-	+	-	-	-
Grip163-NT (1-685 aa)	-	-	+	+	-	-
Grip163-CT (686-1351 aa)	-	-	+	+	-	-
Grip128-NT (1-585 aa)	-	-	-	-	-	-
Grip128-CT (586-1092 aa)	-	-	-	-	-	-

Supplementary Figure 6: Constructs used in Yeast two-hybrid assay. (a) Truncated fragments of Grip and t-Grip proteins used in Y2H assay are indicated. (b) Summary of the interactions (+) and lack of interactions (-) determined by Y2H analysis. Grey cells show interactions also validated by in vitro protein interaction assay.

Supplementary figure 7

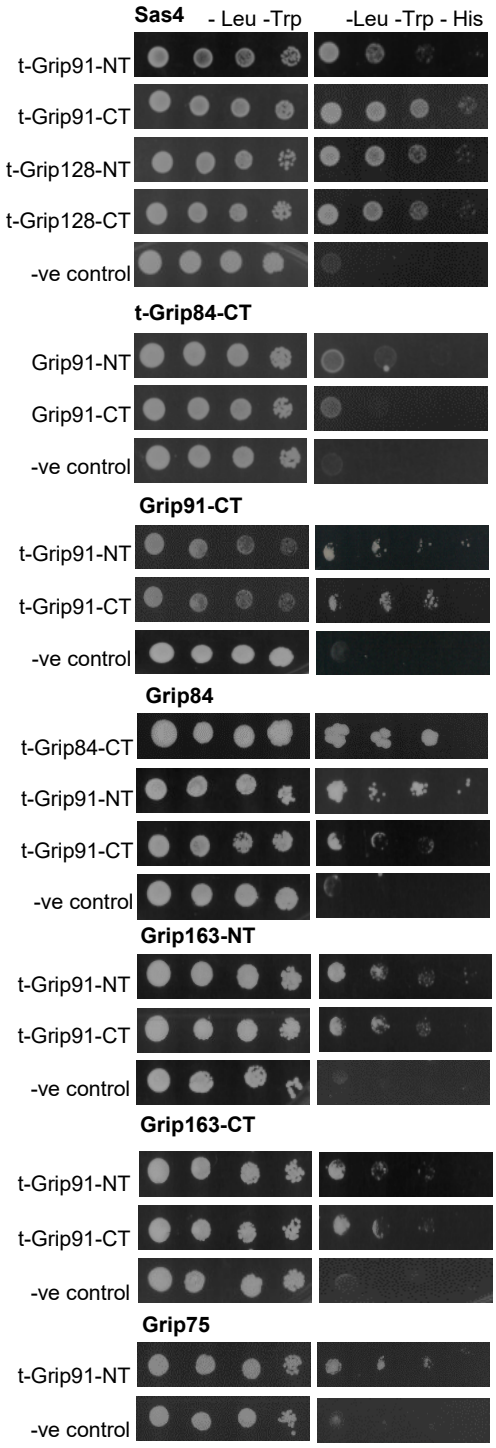

Supplementary Figure 7: Interactions tested by Yeast Two-Hybrid assay
Yeast was plated as 10-fold serial dilutions (left to right) on -Leu, -Trp medium that is selective for the bait and prey plasmids and -Leu, -Trp, -His medium that is selective for the bait, prey, and the interaction between the tested proteins. Negative control (-control) is the empty prey with the corresponding bait vector.

Supplementary figure 8

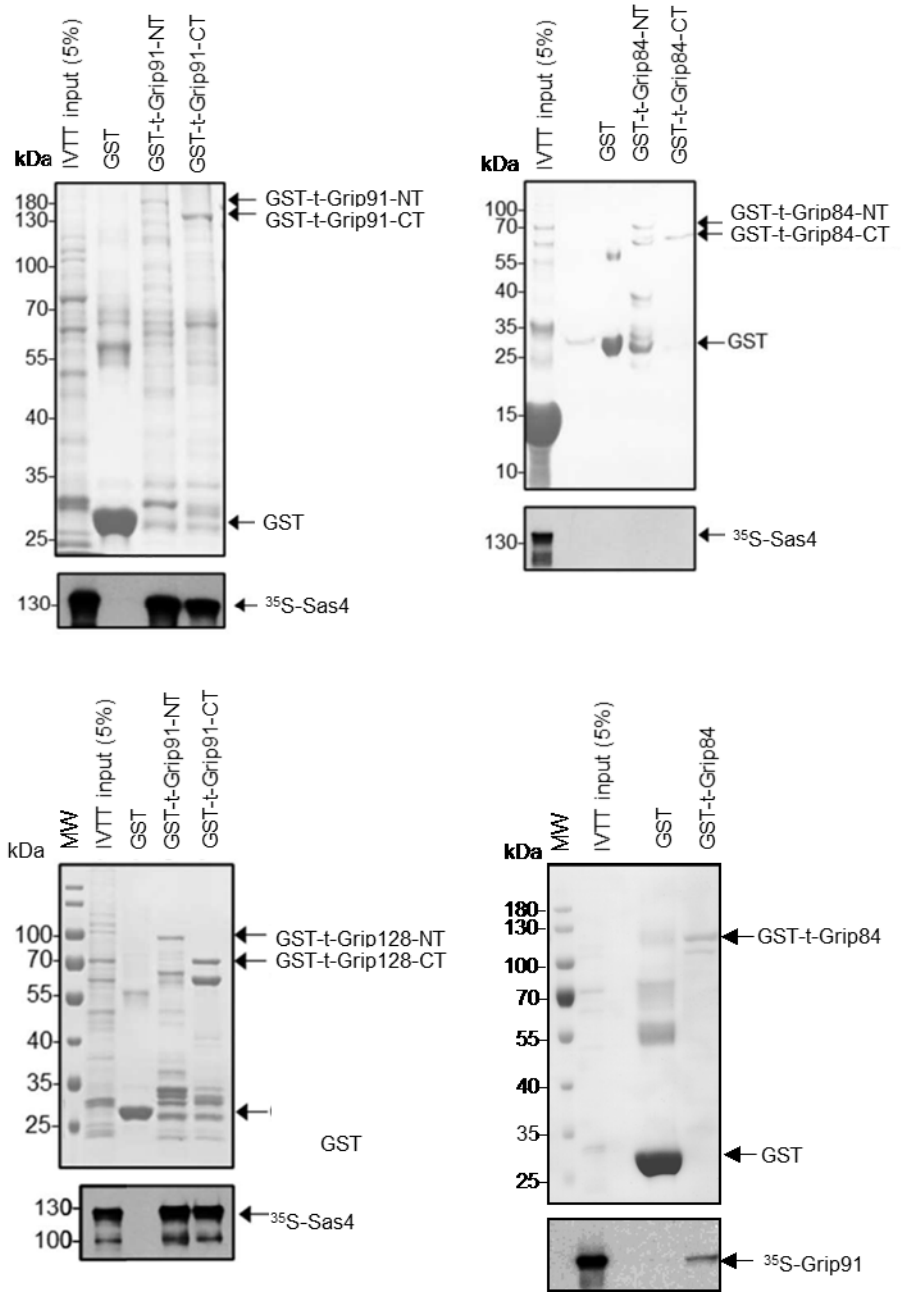

Supplementary Figure 8: Coomassie-Brilliant Blue stained SDS-PAGE gels (upper panel) show the presence of the purified and immobilized GST-t-Grip91-NT, t-Grip91-CT, GST-t-Grip84-NT, GST-t-Grip84-CT, GST-t-Grip128-NT, GST-t-Grip128-CT or full length of t-Grip84 bait proteins used in the in vitro binding assay. Autoradiographs (lower panel) show the 35S labelled IVTT-produced prey proteins (Sas4 and Grip91).

Supplementary figure 9

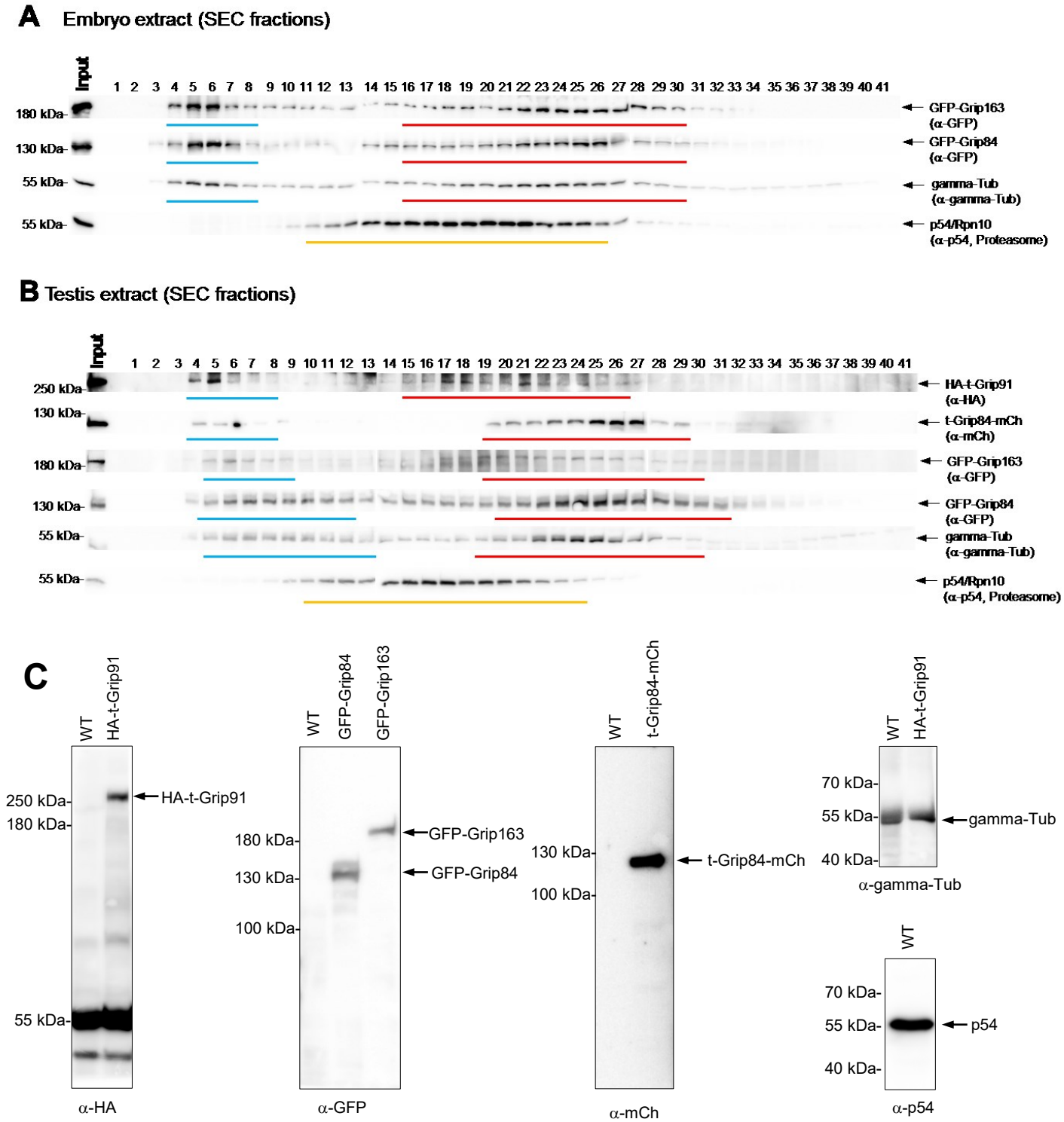

Supplementary Figure 9: Distinct gamma-tubulin-containing complexes are present in Drosophila testis extracts. The separation of different gamma-tubulin-containing complexes in the embryo (a), as well as testes (b) extracts, was carried out by Superose 6 size-exclusion chromatography (SEC). The fractionation pattern of gamma-tubulin, GFP-Grip163, GFP-Grip84, HA-t-Grip91 and t-Grip84-mCh, which were analysed by western blotting using the indicated antibodies, indicates that differently composed gamma-tubulin complexes may present in testes, compared to embryos. Input refers to the sample loaded onto the column. Blue and red bars represent different complexes with different retention profiles. p54/Rpn10 served as a marker of the 26S proteasome (~2.5 MDa). (c) Total protein extracts prepared from testes of wild-type (WT) or transgenic flies were analysed by western blotting using the indicated antibodies.